Cement and Concrete Composites 154 (2024) 105773

Contents lists available at ScienceDirect

Cement and Concrete Composites

journal homepage: www.elsevier.com/locate/cemconcomp

Tailoring of steel fiber surface by coating cellulose nanocrystal for enhanced flexural properties of UHPC

Jiang Du [a,b], Yuhuan Wang [a], Pengwei Guo [a], Weina Meng [a,*]

[a] Department of Civil, Environmental, and Ocean Engineering, Stevens Institute of Technology, Hoboken, NJ, USA
[b] State Key Laboratory of Mountain Bridge and Tunnel Engineering, Chongqing Jiaotong University, Chongqing, 400074, People's Republic of China

ARTICLE INFO

Keywords:
Cellulose nanocrystals
Coating technology
Flexural performance
Fiber dispersion and orientation
Ultra-high-performance concrete

ABSTRACT

Ultra-high-performance concrete (UHPC) is an advanced generation of cementitious composites with excellent compressive strength and durability. However, the relatively poor interfacial transition zone (ITZ) between steel fibers and UHPC matrix leads to insufficient flexural properties and hinders its further applications. This study proposed a cost-effective, sustainable, and highly reactive coating material, cellulose nanocrystals (CNCs), to densify the ITZ of steel fiber surfaces, thus enhancing the flexural properties of UHPC. Utilizing the Herschel-Bulkley model, the critical concentration of 1.0 % is determined for enabling uniform dispersion of CNCs, enhancing the coating performance and reliability. The performance of CNCs as coating materials was evaluated by flexural test of UHPC with CNCs-coated steel fibers, pull-off test, scanning electron microscope (SEM), atomic force microscope (AFM), energy-dispersive spectroscopy (EDS), and Fourier-transform infrared spectroscopy (FTIR). Results showed that compared to UHPC with pristine steel fibers, the flexural strength and toughness of UHPC with CNCs-coated steel fibers were increased by up to 14 % and 18 %, because the single fiber pull-off energy was increased by 50 %. It can be attributed to the densified ITZ which is validated by the increased UHD C-S-H and HD C-S-H on ITZ. However, when the concentration of CNCs suspension (i.e., 1.5 %) exceeds the critical value, the CNCs coating film would stick the uniformly dispersed steel fibers together and then affect their distribution, thus reducing the mechanical performance of UHPC. This work provides a green and effective approach for promoting flexural properties and an in-depth understanding of CNCs coating mechanism.

1. Introduction

Ultra-high-performance concrete (UHPC) is an advanced cementitious composite characterized by self-consolidating property, excellent mechanical strength, and superior durability [1]. According to the standard (ACI 239) [2], the 28-day compressive strength should be higher than 120 MPa under standard curing. Meanwhile, the tensile strength ranges from 7 to 15 MPa, and the strain-hardening can be observed during the post-cracking stages of UHPC specimens [3]. Based on aforementioned excellent performance, UHPC has been extensively employed in various civil construction projects, including precast girders and piles [4–6], cast-in-situ connections and joints [7–12], jackets for columns [13,14], bridge deck overlays [15–23], and reinforcement of damaged bridge arches [24–26]. However, despite its insufficient toughness, some brittle failures still occur when UHPC is exposed to high levels of dynamic loads [27]. The high toughness of UHPC specimens represents the satisfying energy absorption capacity to minimize the brittleness of UHPC infrastructure during the life-span service [28,29].

As shown in Fig. 1(a), under the four-point bending test, the failure of UHPC beams includes elastic stage (Fig. 1(b)), multi-cracks stage (Fig. 1(c)), and localized deformation stage (Fig. 1(d)). The ultimate flexural strength and toughness of UHPC beams are more related to the fiber bridge effect in multi-cracking stage and localized deformation stage, which are determined by the bond behavior between steel fibers and UHPC matrix [30–36]. Therefore, the improvement of interfacial transition zone (ITZ) between steel fibers and UHPC matrix is beneficial for leveraging the synergy of two materials, thus enhancing the flexural performance of UHPC mixtures.

In the past few decades, researchers have extensively studied the interface enhancement between steel fibers and cementitious substrate, including the geometry of the fibers [37,38], densification of UHPC matrix [39,40], and ITZ densification by surface treatment [41,42]. Firstly, several shapes of steel fibers include straight, hooked,

* Corresponding author.
E-mail address: wmeng3@stevens.edu (W. Meng).

https://doi.org/10.1016/j.cemconcomp.2024.105773
Received 19 April 2024; Received in revised form 10 September 2024; Accepted 22 September 2024
Available online 25 September 2024

corrugated, and twisted have been used in the UHPC [37,38,43]. The deformed fibers could increase the mechanical interlock on the interface between steel fibers and UHPC matrix [44]. Specifically, scholars quantified the effect of the steel fiber geometry on the interface bond strength. The bond strengths of corrugated and hooked fibers were 200 % and 600 % higher than that of straight fibers. The flexural strengths of UHPC with corrugated fibers and hooked fibers were 5 % and 20 % higher than that of UHPC with straight fibers [37]. However, two issues still exist for the utilization of deformed steel fibers in UHPC mixtures: (1) the cost of the deformed fibers is much higher than that of straight steel fibers; (2) the use of high-volume deformed fibers might generate split cracks during the pull-out process, which creates weak zones and deteriorates the reinforced effect of adjacent fiber [45]. To densify the interfacial transition zone (ITZ), one of the methods is to densify the entire UHPC matrix. For instance, Shen et al. [39] found that the heat curing is an effective method. As the curing temperature increased from 20 °C to 250 °C, the proportion of ultra-high-density C-S-H in UHPC matrix was increased from 15.4 % to 100 %, which increased the flexural strengths of UHPC matrix by 20 %. However, the heat curing (e.g., steam curing) requires advanced and expensive equipment which is more suitable for precast elements in the concrete plant [1]. Meanwhile, the addition of nanomaterials is also promising [46]. Li et al. [40] investigated the effect nano-SiO_2 addition on flexural performance of UHPC. As the nano-SiO_2 increased to 1.0 %, the 28-day flexural strengths of UHPC were increased by 16 %. Meng and Khayat [47] revealed that, as the carbon nanofiber (CNF) increased from 0 to 0.3 %, the 28-day direct tensile strength were increased by 50 %. However, there still exists some issues on using nanomaterials in UHPC matrix: (1) high cost, for instance, the cost of CNF are around 100–200 $ per kilogram [48,49]; (2) the proper dispersion of nanomaterials for large-scale UHPC production is still problematic [50].

Compared to the densification of the entire UHPC matrix, the improvement focusing on the area around the interfacial transition zone (ITZ) is more straightforward and efficient [30]. Currently, two key factors lead to the weak ITZ: (1) for commercial steel fibers, to prevent the corrosion problems, the surface of steel fibers was planted with the poorly hydrophilic brass. The dezincification of the brass coating would occur in the cement hydration environment, resulting in the destruction of the coating structure and the aggregation of CH [51]; (2) the surface of pristine steel fibers is smooth, lack of physical friction with UHPC matrix [52]. Therefore, the surface modification on steel fibers to enhance the ITZ between steel fibers and UHPC matrix attracted more researchers' interests in the past few years. To enhance the ITZ between steel fibers and UHPC matrix, the following methods were attempted: (1) Physically roughen [53,54], (2) Chemically activate [41,55,56] (3) Nanomaterials coating [42,51,57], as illustrated in Fig. 2. Firstly, Stengel [53] investigated the surface modification on steel fibers using sandpaper with different grits. Results revealed that the bond properties between steel fibers and cementitious matrix were significantly enhanced due to the effect of surface roughness by sandpaper modifications. Besides, Chun et al. [54] pointed out that, compared to steel fibers abraded in the parallel direction, the transversely abraded steel fibers were shown more significant enhancement on the bond properties between steel fibers and cementitious matrix. The major limitation of the sandpaper roughening method is challenging to achieve the large-scale production in the on-site projects. Secondly, the chemical activation aims to introduce the reactive functional groups on surface steel fibers. Miller et al. [41] revealed that plasma is a medium consisting of electrons and positively charged ions, which was extensively used to graft reactive functional groups on the surface of inert fibers. Results indicated that after 8-min oxygen/argon plasma treatment, the wettability of steel fibers was improved and the single-fiber pullout

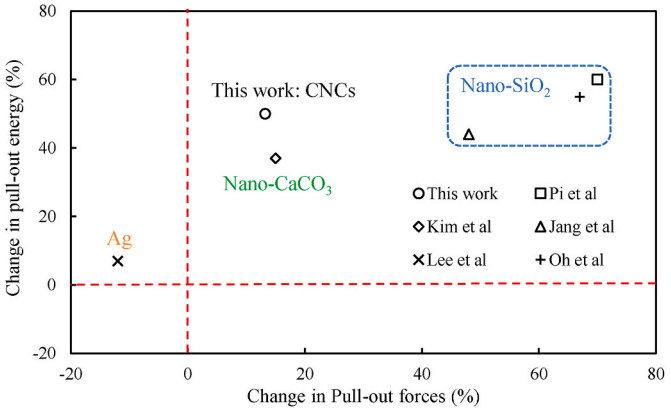

Fig. 2. The relationship between changes in pull-out forces and energies of UHPC with steel fibers modified by different nanomaterials.

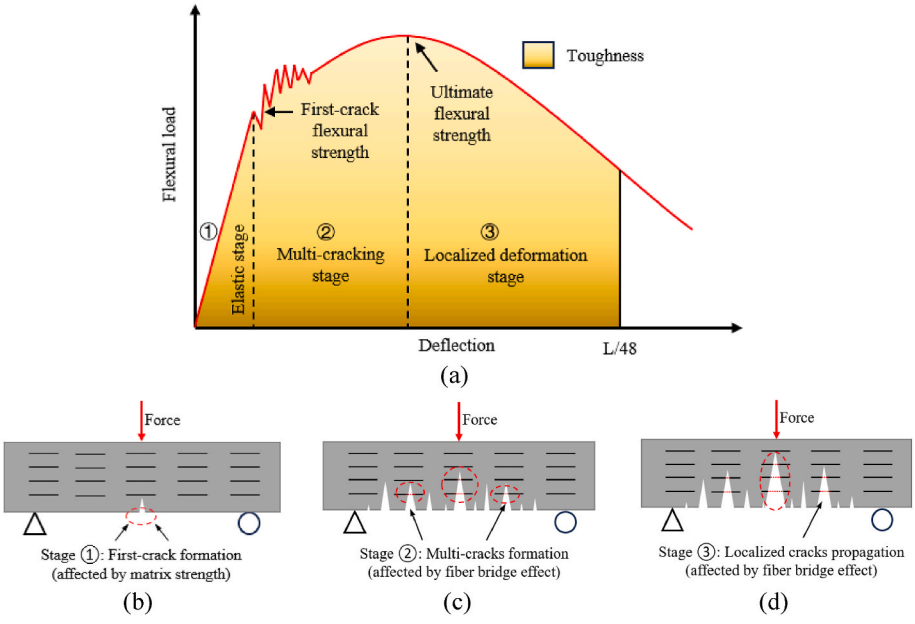

Fig. 1. Flexural properties of UHPC under the bending tests.

energy between the modified steel fibers and concrete matrix were increased by 30 %. Yoo's research group [55,56] studied the chemical surface-roughened modification on steel fibers using an electrolyte-EDTA solution. Results indicated that after 9-h immersion the pull-out energy of straight steel fibers was increased by 39 %. However, it should be noted that the plasma treatment requires specific equipment (e.g., Harrick Expanded Plasma Cleaner PDC-002), and the amount of steel fibers for each treatment are extremely limited (i.e., <20 g) [30]. In addition, Sugama et al. [58] found that, after 15-min ZnPh solution immersion at 90 °C, the pullout load between modified steel fibers and concrete matrix was increased by 40 %, which can be attributed to the formation of hydroxyapatite and brushite on the ITZ and increased roughness [59]. However, the heavy metal ion (Zn^{2+}) and the phosphorus (P) are fatal elements which can pollute water and soil to threaten the environment safety and human health. Most recently, researchers focused on the surface modification of steel fibers by using nanomaterials. Nano-SiO_2 is a promising coating material for steel fibers because the nano-SiO_2 can react with $Ca(OH)_2$ to form hydrated calcium silicate (C-S-H), thus strengthening the ITZ. Pi et al. [60] proposed the sol-gel method to coat nano-SiO_2 film on the surface of steel fibers. Results showed that the pullout energy of modified steel fibers were increased by 70 %. However, the sol-gel coating method is complicated and the initial cost of nano-SiO_2 is still high. In addition to the surface coating method, the chemical solution immersion and sandpaper polishing method were also proposed to roughen the fiber surface [61–63]. Kim et al. [57] investigated the nano-$CaCO_3$ coating on steel fibers for UHPC preparation. Results indicated that the average bond strengths and pull-out energy were increased by 15 % and 37 %. To achieve the uniform nano-$CaCO_3$ modification, EDTA was also added to enable the formation of smaller calcium carbonate particles due to the chelating effect of EDTA. Therefore, it is desperate to propose a more cost-effective and sustainable coating material for steel fibers. the CNCs are proposed as an alternative coating material.

Cellulose nanocrystals (CNCs) are cellulose-based spindle-shaped nanoparticles (3–20 nm in width and 50–500 nm in length) [64]. They are potential candidates to improve the interfacial properties due to the high surface area (≈13 m^2/g) and large amount of hydroxyl groups [65]. Moreover, compared to the traditional nanomaterials (e.g., nano-SiO_2), the CNCs is widely regarded as a type of cost-effective and sustainable material because it can be obtained from numerous natural sources, including crops, agricultural by-products, and forest wood [66]. The cost of CNCs is approximately 50 % lower than that of nano-SiO2 due to the increasing global production volumes, making them more viable for industrial applications [67]. The CNCs have been attempted directly incorporate in the matrix of cement-based composites. it was observed that CNC particles tended to agglomerate, resulting in a decrease in the mechanical performance of these composites [68].

Hence, this study presents a more viable approach for incorporating CNCs into cementitious composites by applying a coating to the surface of steel fibers. To date, the CNCs have been employed to improve the bond performance at the interface between epoxy and glass fibers [69,70]. Results showed that the interfacial shear strength between epoxy and glass fiber was increased by 60 % and the flexural strength of the glass fiber-epoxy composite was increased by 40 %. The underlying mechanism for the enhancement in bond performance is that the glass fibers carry the reactive hydroxyl groups which can generate strong hydrogen bond with CNCs at interface [70]. Previous studies proved that CNCs is the potentials coating materials to enhance the interface. However, to date, there is still lack of knowledge on the steel fiber coating by CNCs particles because the following challenges are yet to be addressed: (1) Very few hydroxyl groups can be found on the surface of copper-coated steel fibers. How can the pristine steel fibers be effectively coated by CNCs? (2) The CNCs suspension is prone to agglomerate when the concentration is high. How to determine the optimal concentration of CNCs suspension for coating steel fibers? (3) What is the performance and mechanisms of CNCs-coated steel fibers on UHPC? (4) How does the CNCs coating affect the ITZ between steel fibers and UHPC matrix? What is the variance on the ITZ between CNCs-coated steel fibers and UHPC matrix?

To answer the above questions, the objectives of this research include: (1) to proposes a cost-effective and sustainable method to effectively coat CNCs on surface of steel fibers; (2) to determine the critical concentration of CNCs suspension on coating steel fibers; (3) to investigate the mechanical properties of UHPC with CNC-coated steel fibers and elaborate the underlying mechanisms; (4) to quantify the microstructure of ITZ between CNCs-coated steel fibers and UHPC matrix. The SEM-EDS, AFM, contact angle measurement, and FT-IR are conducted to characterize the coating effect of CNCs on steel fibers. The flowability, mechanical properties, and autogenous shrinkage are conducted to characterize the CNCs coating effect on performance of UHPC itself. The microscale mechanical analysis (i.e., nanoindentation) on ITZ is conducted to explain the underlying mechanism of CNC coating for UHPC. This research can facilitate the wilder application of UHPC in civil infrastructures.

2. Raw materials, coating process, and mixture design

2.1. Raw materials

The UHPC mixture is composed of binder materials, fine aggregates, steel fibers, tap water, and high-range water reducer (HRWR). Type I Portland cement and ground granulated blast-furnace slag (GGBFS) from a local plant in New Jersey were employed as binder materials. River sand was used as fine aggregates. The chemical compositions of the dry ingredients were characterized by X-ray fluorescence (XRF) and X-ray diffraction (XRD), listed in Table 1. Besides, cellulose nanocrystals (CNCs) are purchased from CelluForce.

Besides, the particle size distribution curves of the cement, GGBFS, and river sand are shown in Fig. 3. The pristine steel fibers measuring 0.2 mm in diameter and 13 mm in length were incorporated. The tensile strength and elastic modulus are 1.9 GPa and 203 GPa, respectively. To ensure the proper workability, a polycarboxylate-based HRWR was used. The solid content and specific gravity were 34.4 % and 1.05, respectively.

The TGA analysis, particles size distribution, and TEM images of the CNC morphology were conducted and elaborated. For the chemical composition, the mass loss of CNCs is analyzed at three levels of temperature shown in Fig. 4(a): (1) 30–200 °C: the evaporation of water; (2) 200–600 °C: the dehydration and decomposition of CNCs; and (3) 600–1000 °C: the aromatization of CNC. In addition, Fig. 4(b)–**(c)** show the dynamic particle size distribution and morphology of CNCs. The dynamic particle size of the CNCs was measured to be approximately

Table 1
Chemical and physical properties of raw materials.

	Type I Portland cement	GGBFS	River sand
SiO_2 (%)	22.44	36.21	86.50
Al_2O_3 (%)	2.76	11.10	0.39
Fe_2O_3 (%)	2.24	0.76	1.47
CaO (%)	68.05	43.75	9.42
MgO (%)	0.91	5.09	–
SO_3 (%)	2.25	2.21	–
Na_2O (%)	0.19	0.23	–
K_2O (%)	0.11	0.40	–
TiO_2 (%)	0.14	0.58	–
P_2O_5 (%)	0.09	0.02	–
Mn_2O_3 (%)	0.03	0.36	–
C_3S (%)	62.35	–	–
C_2S (%)	20.28	–	–
C_3A (%)	1.42	–	–
C_4AF (%)	5.83	–	–
Loss on ignition (%)	1.28	0.72	0.24
Specific gravity	3.15	2.90	2.64

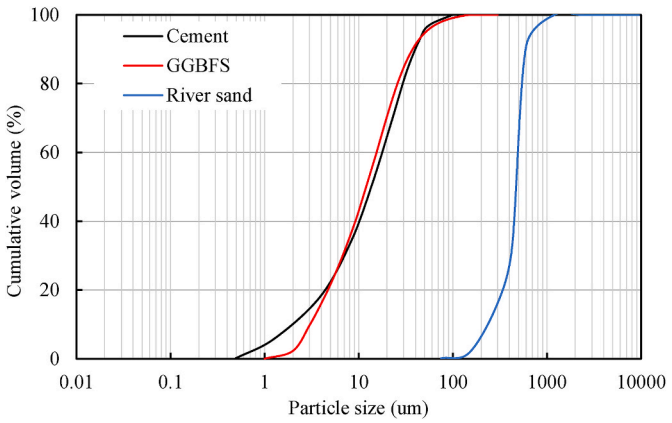

Fig. 3. Particle size distribution of dry raw materials.

100 nm, and the CNCs exhibit a rod-like morphology, with lengths ranging from 100 to 200 nm and diameters between 5 and 10 nm.

2.2. Steel fiber coating process

The as-received CNCs materials were in form of freeze-dried powder. Thus, 30 min of sonication was performed to well disperse the CNCs in DI water, accompanying an ice water batch to minimize the possible desulfation [71,72]. In this study, nine CNCs suspensions with different concentrations were investigated (e.g., from 0.25 % to 3.0 % by volume of DI water). Their dispersion effect and rheological properties were evaluated in Section 4.1.

Subsequently, a serial of simple and appropriate treatment action was adopted to obtain the satisfactory coating effect on surface of steel fibers [28,73]. Specifically, the CNCs coating process can be mainly divided into two steps: (1) Step 1: pristine steel fibers were immersed in NaOH solution (the concentration is 20 %) for 30 min to enhance the surface activity. Then, the steel fibers were washed with the deionized water and ethyl alcohol to remove the residual NaOH solution. After the pretreatment, large amounts of hydroxyl groups (i.e., -OH) was introduced onto the surface of steel fibers, which contributes to the coating of CNC particles. (2) Step 2: the pretreated and dried steel fibers were immersed into the corresponding CNC suspension for 1 h, and then dried in an oven at 40 °C for 24 h. Finally, the coated steel fibers were properly stored and ready for casting UHPC specimens. The schematic diagram of the coating progress is shown in Fig. 5(a). More importantly, the coating mechanism is the hydrogen bonding between the hydroxyl groups (i.e., -OH) on the CNCs particles and steel fiber surfaces [74], shown in Fig. 5 (b).

2.3. Mixture design

All investigated UHPC mixtures in this study is given in Table 2, based on the cost-effective UHPC mixtures in previous research [75]. The binder-to-sand ratio was fixed at 1:1 by volume and the water-to-binder ratio was fixed at 0.23 by mass. The control mixture

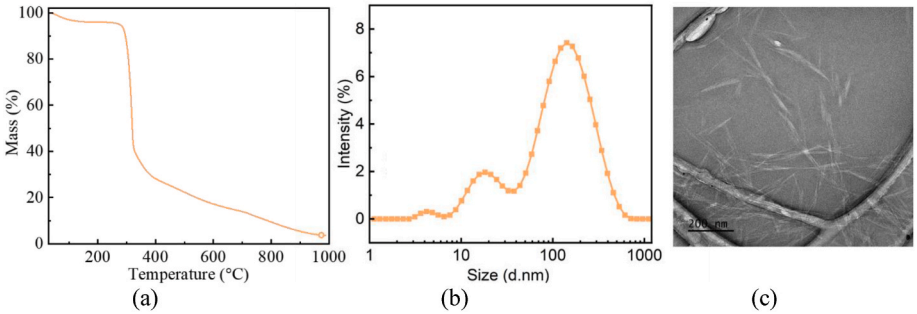

Fig. 4. Characterization of CNCs: (a) FTIR spectrum, (b) dynamic particle size distribution, and (c) TEM image showing the morphology of CNCs.

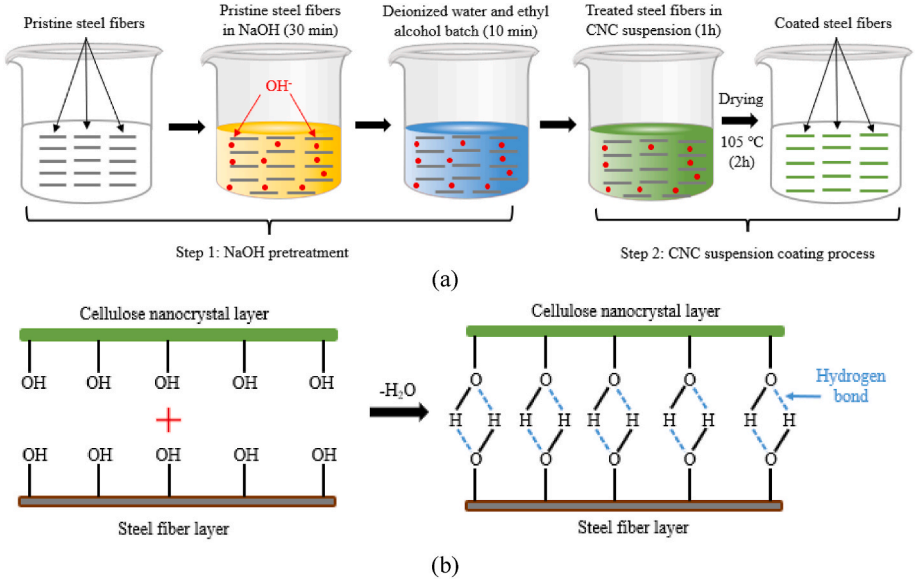

Fig. 5. The schematic diagram of: (a) CNCs coating progress; (b) CNCs coating mechanism.

Table 2
Mixture proportions of UHPC (kg/m^3).

Mixture	Cement	GGBFS	River sand	HRWR	Water	PSF	CSF
Control	459.0	633.9	965.4	8.0	248.1	156.0	–
0.5CSF	459.0	633.9	965.4	8.0	248.1	–	156.0
1.0CSF	459.0	633.9	965.4	8.0	248.1	–	156.0
1.5CSF	459.0	633.9	965.4	8.0	248.1	–	156.0

Note: HRWR represents high-range water reducer, PSF represents pristine steel fibers, and CSF represents coated steel fibers.

represents the UHPC mixture reinforced with 2 % pristine steel fibers. In addition, the 0.5CSF mixture represents the UHPC mixture reinforced with 2 % CNCs-coated steel fibers, and the steel fibers are coated with a CNCs suspension with a 0.5 % concentration by mass.

3. Experimental methods

3.1. Mixing and specimen preparation

The UHPC mixer (model: Hobart® HL-200) was used to homogenize raw materials for the UHPC production. The mixing procedures developed in previous research were adopted in this study, including four steps: (1) cement, GGBFS, and river sand are added into the mixer and mixed at 107 RPM for 2 min (2) HRWR is dissolved into the tap water to form a solution, and 90 % of the solution is added into the mixer at 107 RPM for 3 min (3) the remaining 10 % solution is added into the mixer at 107 RPM for 3 min (4) steel fibers are added to the mixer at 198 RPM for 2 min. After mixing, the homogenized UHPC mixtures were examined by hand, and no fiber agglomeration or segregation was found.

Subsequently, fresh UHPC mixtures were used to cast cubic specimens for compressive test, beam specimens for flexural test, and prism specimens for shrinkage test. Immediately after casting, the specimens were covered by wet burlap and plastic sheet to prevent the moisture loss. The specimens were demolded after 1 day, and then cured in lime-saturated water at room temperature (23 ± 2 °C) until testing.

3.2. Rheology of CNCs suspension

Rheological experiments were conducted to quantify the dispersion and agglomeration of CNCs in DI water. The Anton Paar MCR 302 rheometer was applied to evaluate rheological properties of CNCs suspension, shown in Fig. 6. The testing geometry consisted of 25-mm concentric cylinder systems with sandblasted surface, which prevents the slippage [76]. All CNCs suspension with different concentrations were conducted after 30-min sonification.

Subsequently, the equilibrium flow curve method was applied to evaluate the rheological properties. Detail procedures were shown below: (1) the CNCs suspension was pre-sheared at 250 s^{-1} for 30 s; (2) the shear rate was stepwise from 250 s^{-1} to 200 s^{-1}, 150 s^{-1}, 120 s^{-1}, 90 s^{-1}, 70 s^{-1}, 50 s^{-1}, 40 s^{-1}, 30 s^{-1}, 20 s^{-1}, and 10 s^{-1}. For each step, the shear rate was kept for 10 s (Fig. 7(a)); (3) the steady state of the shear stress was fitted by the Herschel-Bulkley model (Fig. 7(b)); (4) the yield stress, consistency, and flow index were calculated.

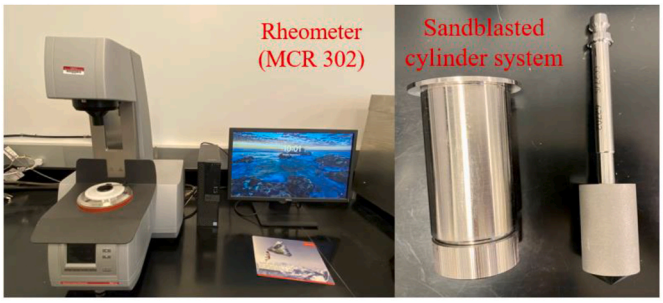

Fig. 6. The rheology test equipment: Anton Paar MCR 302 rheometers.

3.3. Characterization of UHPC with CNCs-coated steel fibers

3.3.1. Fresh and hardened properties

The workability of the UHPC mixture was evaluated through mini-slump flow test, in accordance with ASTM C230 [77]. All test results were repeated three times to ensure the reproductivity. The mini-slump flow test was shown the self-consolidating property.

The compressive strength was evaluated through uniaxial compressive tests using 50-mm cubes, in accordance with ASTM C109 [78]. The loading rate was kept constant at 1.8 kN/min. The compressive tests were conducted at 1, 3, 7, and 28 days.

The flexural properties were evaluated through four-point bending tests in according with ASTM C1609 [79]. The test specimens measured 280 mm × 76 mm × 76 mm. The loading span length was 94 mm. The bending tests were conducted using a load frame (model: Instron® 5982) under displacement control. The displacement rate was 0.05 mm/min. The tests were performed to evaluate the flexural strength and energy dissipation at 7 d and 28 d. The flexural strength was calculated using Eq. (1). In addition, the area between the load-deflection curve and horizontal axis (from 0 to L/48 = 5 mm) is the calculated toughness of UHPC specimens.

$$\sigma = \frac{3F(L - L_i)}{2bd^2} \quad (1)$$

where F, L, L_i, b, and d are the peak load, distance between supports (L = 240 mm), distance between loads (L_i = 94 mm), beam width, and beam depth, respectively.

3.3.2. Hydration heat

The heat of hydration of each mixture (with steel fibers) was evaluated using an isothermal calorimeter (model: Calmetrix® I-Cal 4000 HPC), which was programmed to maintain the sample at 25 °C. Approximately 60 g of fresh UHPC mixtures, incorporating either pristine or CNCs-coated steel fibers, were sealed in plastic vials and placed in the calorimeter. Considering the difficulty of precisely controlling fiber numbers in each vial, only 0.3 L fresh UHPC were prepared and then filled into three individual plastic vials for the calorimeter test to ensure the relatively fair comparison. Finally, the hydration heat was measured continuously from 2 min post-mixing up to 48 h, and the results were normalized to the mass of the binder.

3.3.3. Single fiber pull-out test

The single fiber pull-out test was performed using a customized setup, shown in Fig. 8. During the casting process, the pristine and CNCs-coated steel fibers measuring 13 mm in length were embedded in 50-mm cubic specimens which were tightly restrained by the steel frame system shown in Fig. 8(a). When steel fibers started to be pulled out, the force load and the pull-out displacement were simultaneously measured by the load cell (Max: 500 N) and a LVDT was embedded in the load frame (Model: Instron 5982 Universal Testing Systems), shown in Fig. 8(b). The single fiber pull-out test was performed under the displacement control mode at the rate of 0.5 mm/min. Three identical steel fibers were embedded on each cube specimen. Specifically, a 6-mm length was embedded into the UHPC matrix and a 4-mm length was gripped by the load frame for applying tensile forces.

3.3.4. Interfacial transition zone characterization

The morphology of the interfacial transition zone (ITZ) between pristine/CNCs coated steel fibers and UHPC matrix was observed by scanning electronic microscope (model: Zeiss Auriga FIB/SEM with a SE2 detector), and the accelerating voltage was 5.0 kV. In order to further quantify the micro-mechanical properties in the ITZ areas, the

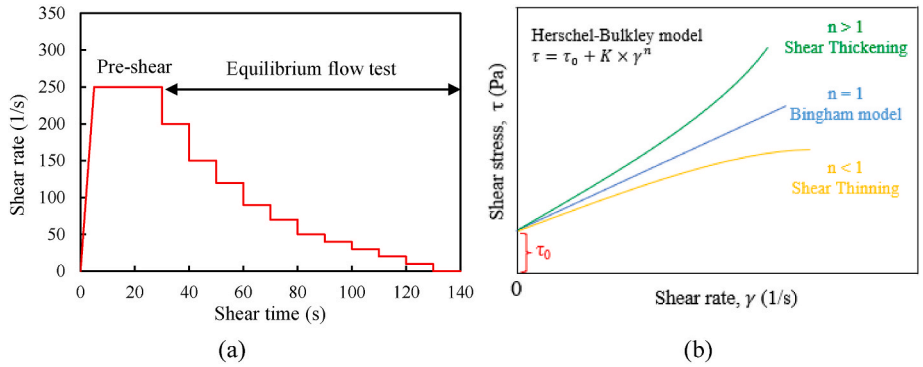

Fig. 7. The protocol to determine rheology of CNCs suspension: (a) equilibrium flow curve (b) the Herschel-Bulkley model.

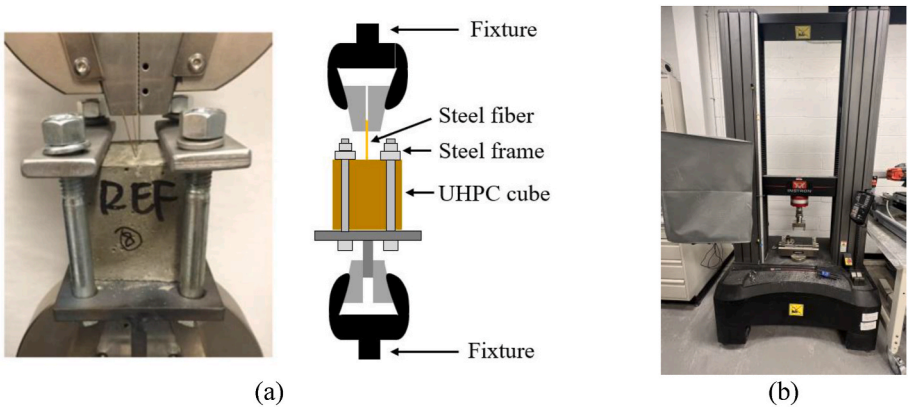

Fig. 8. Test setup and specimens of the single fiber pull-out test: (a) the steel frame system; (b) single fiber pull-out load cell and LVDT measurement.

AFM-based nanoindentation was conducted to characterize the phase composition of the ITZ around the steel fibers. The sample preparation process for the AFM-based nanoindentation test were shown below: (1) after 28 days curing, UHPC samples were cut into pieces and soaked in isopropanol to stop further hydration, then vacuum dried for 24 h; (2) the dried UHPC samples were deposited in a rubber mold and sealed with epoxy resin; (3) the surface was polished using abrasive papers (#400, #600, #800, and #1200) on a polish machine (model: Met Prep 3M polisher); (4) the surface was polished using 1 μm polycrystalline diamond suspension and 0.05 μm FinalPrep Alumina polish solution on a Diamat polishing cloth; (5) each sample was washed with ethanol to remove impurities.

Peak-Force quantitative nanomechanics (QNM) was applied to evaluate the elastic modulus of samples using an atomic force microscope (AFM, model: Bruker Bioscope Resolve AFM with integrated fluorescence microscope). The produces are showing below, a probe advanced towards the sample surface, exerted indentation to a specific depth, and subsequently withdrew into the air. Throughout this procedure, the mechanical response of the localized area was monitored to assess the elastic modulus. The elastic modulus was then computed using Eq. (2) and Eq. (3) [80].

$$F^{2/3} = \left(\frac{4}{3}\frac{E^*}{(1-\upsilon^2)}\sqrt{R}\right)^{2/3}\delta \tag{2}$$

$$E^* = \left[\frac{1-\nu_p{}^2}{E_p} + \frac{1-\nu_s{}^2}{E_s}\right]^{-1} \tag{3}$$

where F, representing the tip force measured from the AFM probe; E* represents the reduced modulus of the tip and sample; υ represents the Poisson's ratio of the tip and sample; R is the radius of the probe; δ is the indentation depth; ν_p and ν_s are the Poisson's ratios of the probe and the sample, respectively; and E_p and E_s represents the elastic moduli of the probe and the sample, respectively. The Nanoscope software was employed for the calculation of the elastic modulus.

Three samples from different sections of UHPC specimens were used for the nanoindentation tests. Besides, all indentations were performed at room temperature (i.e., 25 °C) with a diamond probe (DNISP-HS, Bruker) with a stiffness of 360 N/m and a tip radius of 40 nm. The deflection sensitivity was calibrated using a sapphire substrate. The Poisson's ratio of the probe was 0.33. The elastic modulus of the probe is far higher than that of the samples, so Eq. (2) is rewritten as Eq. (4). The position and distribution of indentation points at the interface between

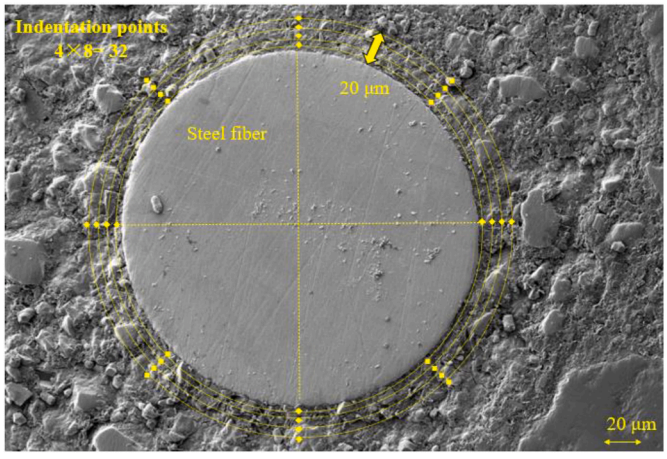

Fig. 9. The schematic diagram of indentation points at the interface between UHPC matrix and steel fibers.

steel fiber and UHPC matrix were shown in Fig. 9. Moreover, for each indentation point, the AFM scanned a 1 μm × 1 μm area with the scanning resolution of 256 × 256. Hence, this configuration resulted in a total of 256 × 256 measurements obtained from each indentation point. The mean elastic modulus of each indentation point was obtained using the Nanoscope software.

$$E^* = \frac{E_s}{1 - \nu_s{}^2} \tag{4}$$

3.4. Characterization of CNCs-coated steel fibers

The surface morphology of pristine and CNCs-coated steel fibers was simultaneously analyzed by scanning electronic microscope (SEM) and atomic force microscope (AFM). SEM images were acquired from the Zeiss Auriga FIB/SEM, and the accelerating voltage was 5.0 kV. In addition, the elements content on steel fiber surface were recorded by the point scanning method of energy dispersive spectrometer (EDS). AFM measurement was conducted using the Bruker ICON AFM, with the scan size of 5 μm × 5 μm and the scan rate of 1 Hz, which uses a probe with a spring constant of 0.8 N/m and a resonant frequency of 95 kHz.

The variations of chemical composition on surface of pristine and CNCs-coated steel fiber were analyzed by Fourier-transform Infrared Spectroscopy (FTIR), which was tested by FT-IR spectrometer (model: Thermo Nicolet Nexus 670) equipped with ATR microscope. The wavenumber ranging from 500 cm^{-1} to 4000 cm^{-1} was selected.

The wettability of pristine and CNCs-coated steel fibers was evaluated by the contact angle test, which were measured by the goniometer (model: Rame-hart 500). At least ten fibers were studied to ensure the reproductivity of results.

4. Experimental results

4.1. Determination of CNCs concentration

The distribution and agglomeration of the CNCs is related to the CNCs concentrations in different solution [81]. Cao et al. [68] found that, as the concentration of CNCs exceeds 1.35 % by volume in DI water, CNCs start to agglomerate, however, the CNCs start to agglomerate when the concentration of CNCs just reaches to 0.18 % in simulated cement paste pore solution. Moreover, the agglomerated CNCs highly affected the microstructural and mechanical properties of cement paste matrix [68]. Therefore, this research firstly determinates the critical concentration of used CNCs in DI water by investigating the rheological properties of CNCs suspension. At low concentrations (Stage I), the CNCs particles are mostly well-dispersed in the DI water and therefore have high mobility [68]. However, with the increasing of CNCs concentration, more CNCs particles are prone to form agglomeration or network structures, which results in the gelation of CNCs suspension (Stage II) [82]. Fig. 10(a) plots the shear stress - shear rate curves for CNCs suspension with concentrations ranging from 0 to 3.0 %. In general, based on the Herschel-Bulkley model, the aqueous CNCs suspension shows a shear-thinning behavior, especially for the higher CNCs concentrations.

The flow index (n) strongly correlates with CNCs concentrations and is an indicator of the agglomeration of CNCs suspension [68]. Fig. 10(b) plots the relationship between the flow index and CNCs concentrations. Results shows that the flow index (n) was kept at a plateau (i.e., n = 1) until the CNCs concentration reaches 1.0 %. With the CNCs concentration exceeding 1.0 %, the flow index decreased below 1 and the CNCs suspension changed from Newtonian fluid to non-Newtonian fluid (shear thinning property), shown in Fig. 10(c). The underlying mechanism is the alignment, ordering, and agglomerates of the CNCs particles in the DI water [83]. This suggests that, for CNCs concentrations above 1.0 %, the CNCs particles start to form the agglomeration. Therefore, in this study, the percolation threshold of CNCs concentration is determined as 1.0 %.

4.2. Characterization of UHPC with CNCs-coated steel fibers

4.2.1. Fresh properties

The workability of UHPC mixtures is the key parameter to affect the construction quality. Poor workability leads to the poor compaction and is hard to achieve placement [84,85]. In this study, the workability of

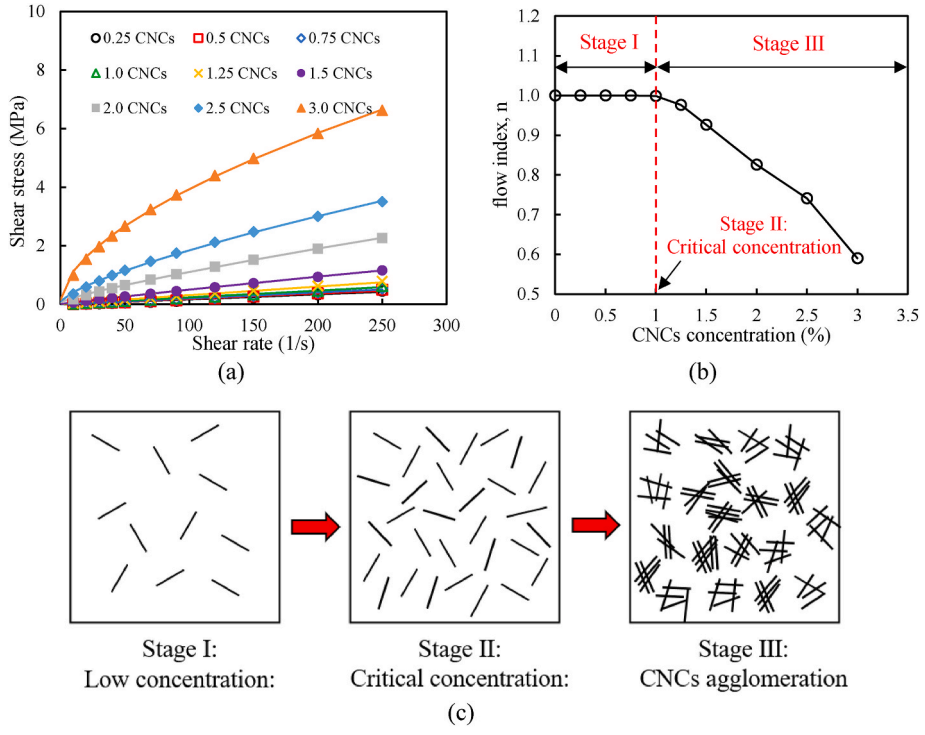

Fig. 10. The shear stress and shear rate curves of CNC suspension at different concentrations.

UHPC mixtures with pristine and CNCs-coated steel fibers was evaluated by the mini-slump flow test. Fig. 11 plots the mini slump spread of investigated UHPC mixtures. Specifically, compared to the control mixture, the mini-slump diameter of 1.5CSF was decreased from 275 mm to 230 mm (by 16 %) and air content of 1.5CSF was increased from 2.9 % to 4.9 % (by 65 %). Results indicated that the utilization of CNCs-coated steel fibers would reduce the flowability of UHPC mixtures. It was speculated that the CNCs coating film (especially in the higher CNCs concentration) might lead to the agglomeration of steel fibers, thus reducing the workability of UHPC mixtures, which was discussed in Section 5.

4.2.2. Compressive strength

The compressive strength of UHPC mixtures is one of the key factors to determine its excellent performance. Fig. 12 plots the compressive strengths of investigated UHPC mixtures from 1 day to 28 days. Specifically, compared to the control mixture, the 3-day and 28-day compressive strengths of 1.0CSF were increased from 70.2 MPa to 79.8 MPa (by 14 %) and from 121.9 MPa to 127.8 MPa (by 5 %). It is speculated that the CNCs coating enhances the physical and chemical bonds between steel fiber and matrix, which is discussed in section 5.1.

However, the compressive strength of UHPC decreased instead when using steel fibers modified by a CNCs suspension at a concentration of 1.5 %. For instance, compared to the control mixture, the 28-day compressive strengths of 1.5CSF were decreased from 121.9 MPa to 116.3 MPa (by 5 %). Results revealed that the utilization of CNCs-coated steel fibers can efficiently improve the compressive strength of UHPC, but the steel fibers coated by CNCs suspension at a high concentration (i.e., 1.5 %) exceeding the critical concentration (i.e., 1.0 % in this study) would undermine the compressive performance of UHPC instead. It was speculated that: (1) compared to the control mixture, the air content of 1.5CSF was significantly increased, which weakened the densified UHPC matrix and reduced the compressive strength; (2) when the concentration of CNCs suspension is higher than the critical concentration, the CNCs coating film led to the severe agglomeration of steel fibers and then reduce the compressive strength, which was quantified in Section 5.2.

4.2.3. Flexural performance

Fig. 13 plots the flexural performance results of investigated UHPC mixtures at 7 days and 28 days. Fig. 13(a) and **(b)** shows the representative flexural strength-deflection curves. Fig. 13(c) summarized the results of average flexural strengths and toughness. Compared to the control mixture, the 28-day flexural strengths and toughness of 1.0CSF were increased from 23.5 MPa to 26.7 MPa (by 13.6 %) and from 106.6 N mm to 125.1 N mm (by 17.3 %). Besides, the flexural performance of UHPC also decreased when using steel fibers modified by a CNCs suspension at a concentration of 1.5 %. For instance, compared to the control mixture, the 28-day flexural strength and toughness of 1.5CSF were decreased from 23.5 MPa to 22.3 MPa (by 5 %) and from 106.6 N mm to 105.1 N mm (by 3 %). For all UHPC mixtures, both the pristine and CNCs-coated steel fibers were pulled out from UHPC matrix after the flexural tests.

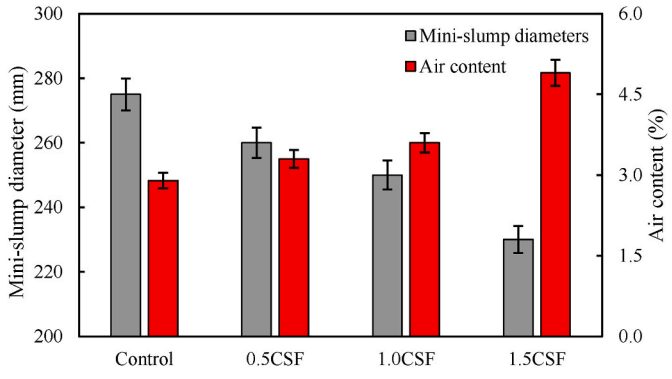

Fig. 11. Results of mini-slump spread for UHPC with pristine and CNCs-coated steel fibers.

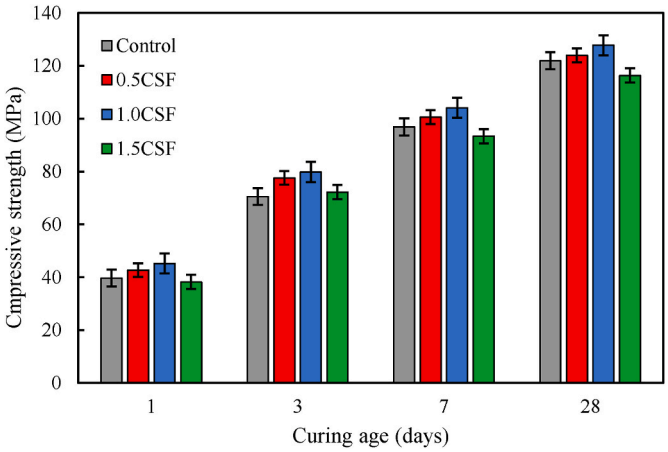

Fig. 12. Results of compressive strengths for UHPC with pristine and CNCs-coated steel fibers.

The similar phenomenon was observed in both compressive and flexural properties that pristine steel fibers coated by proper concentration of CNCs suspension would help enhance the mechanical performance and pristine steel fibers coated by excessive concentration of CNCs suspension reduces the mechanical performance instead. In addition to the negative effect from the high air content mentioned in Section 4.3.2. The underlying mechanisms about the performance enhancement and reduction are clearly elaborated in Section 5.

4.2.4. Single-fiber pull-out test

Fig. 14 plots the single fiber pull-out results of investigated UHPC mixtures. Fig. 14(a) plots the pull-out force-slip curves and Fig. 14(b) plots the summarized max force and absorbed energy. The interface bond between the steel fiber and the UHPC matrix is composed of chemical adhesive bond, friction, and mechanical interlock effect [86]. The single fiber pull-out test can directly reveal the effect of CNCs coating effect on the bonding strength and help to elaborate the enhancement of the flexural performance of UHPC. Result showed that the CNCs coating film monotonically increased the bond strength between UHPC matrix and steel fibers. For instance, compared to the control mixture, the max force and energy of 1.5CSF were increased from 47.0 N to 53.2 N (by 13.2 %) and from 126.8 mJ to 182.3 mJ (by 50 %), respectively. These can be attributed to: (1) The CNCs coating effectively increased the roughness of steel fiber surface, thus enhancing the mechanical interlock effect; (2) The CNCs coating introduced lots of reactive functional group (e.g., -OH) to enhance the reactivity and hydrophilicity of steel fiber surface, thus enhancing the chemical adhesive bond. These mechanisms are elaborated in Section 5.1. In summary, the CNCs coating efficiently improved the matrix-steel fiber interface.

4.2.5. Hydration heat

Fig. 15 plots the isothermal calorimetry results of investigated UHPC mixtures with pristine and CNCs-coated steel fibers. The hydration heat evolution of UHPC mixtures helps to explain the enhancement of mechanical strength, especially at early ages. Specifically, results in Fig. 15 (a) showed that, compared to the control mixture, the peak time of the heat flow of 1.5CSF was advanced from 11.5 h to 9.5 h (by 17.3 %). Results indicated that the utilization of CNCs-coated steel fiber can efficiently promote and accelerate the hydraulic reaction of investigated mixtures, which helps validate the mechanical strength enhancement in Section 4.2.2 and Section 4.2.3. The reason is that CNCs enhance cement hydration in the interfacial transition zone (ITZ) by facilitating water

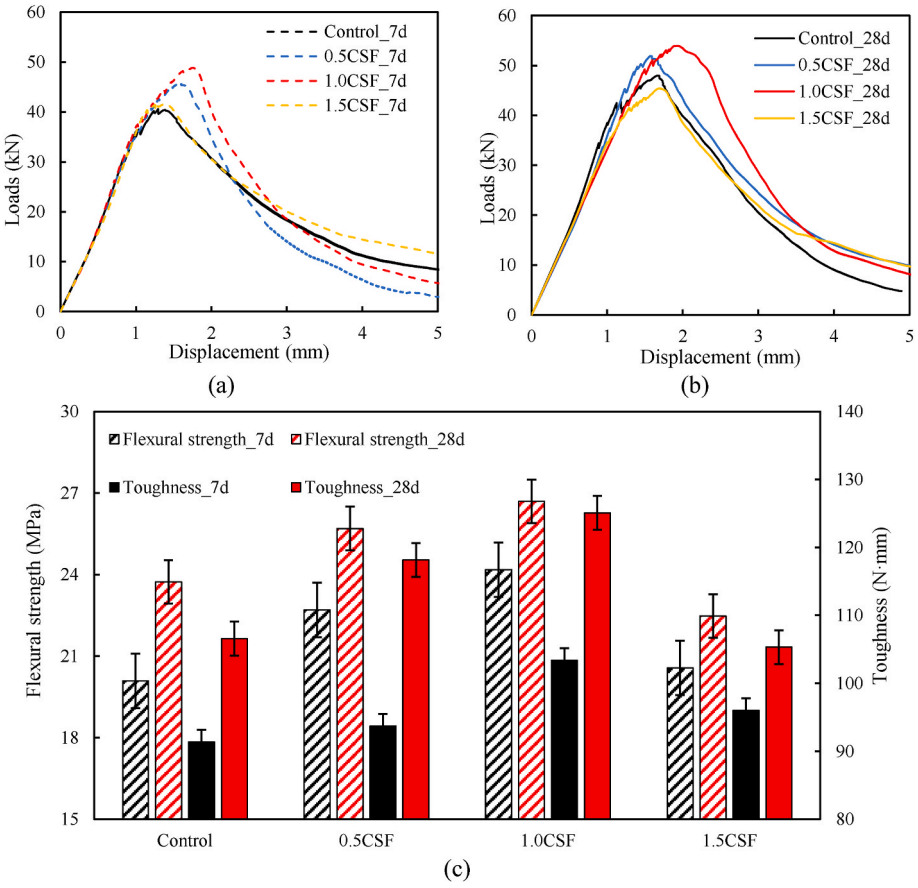

Fig. 13. Results of flexural performance for UHPC with pristine and CNCs-coated steel fibers: (a) load-deflection curves at 7 days; (b) load-deflection curves at 28 days; (c) summarized flexural strengths and toughness.

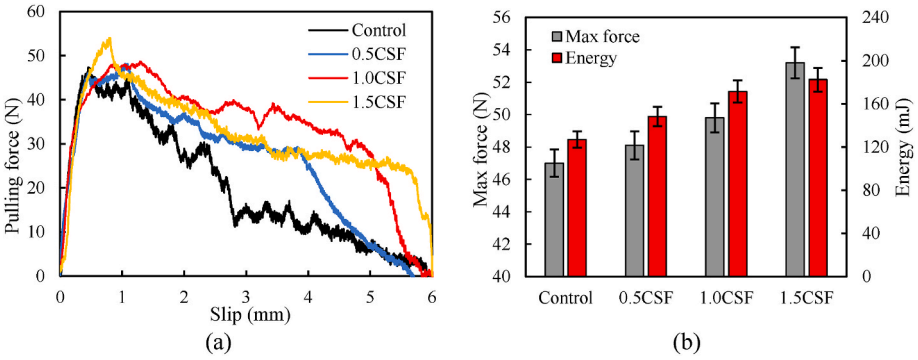

Fig. 14. Results of single fiber pulling-out test for pristine and CNCs-coated steel fibers: (a) pulling force-slip curves; (b) summarized max force and absorbed energy.

transport from pore water to unhydrated cement cores in the ITZ, shown in Fig. 15(b) [80,81,87].

4.2.6. Interfacial transition zone (ITZ) characterization

The micromechanical properties of the ITZ between UHPC matrix and pristine or CNCs-coated steel fibers were quantitatively evaluated through the nanoindentation analysis, which is a well-established technique to study the mechanical response of materials at microscale [73]. For the UHPC with CNCs-coated steel fibers, the mixture (1.5CSF) was investigated in this section. Fig. 16(a) plots the results of the elastic modulus of all indentation points, and these data were shown by cluster allocation. Preliminary investigation through SEM test (shown in Fig. 16 (b)) observed the loose ITZ between the pristine steel fibers and UHPC matrix. In comparison, the ITZ between the CNCs-coated steel fibers and UHPC matrix is much denser.

In order to quantify the ITZ quality, the proportion of phase component of ITZ was studied. The ITZ consists of pores, hydration products, and anhydrate clinkers. Besides, the hydration products are mainly divided as low density (LD) C-S-H, high density (HD) C-S-H, and ultra-high density (UHD) C-S-H, respectively. According to the previous research, the reduced modulus values of pores, LD C-S-H, HD C-S-H, UHD C-S-H, and clinkers are in the range of 0–13 GPa, 14–25 GPa, 25–40 GPa, 40–60 GPa, and over 60 GPa [88,89]. Therefore, the phase proportions of the ITZ for pristine steel fibers and CNCs-coated steel fibers were calculated and shown in Fig. 16(b). Specifically, after the CNCs coating process, the region of indentation points showed that the clinker phase significantly decreased as well as the HD C-S-H and UHD C-S-H phase dramatically increased. This trend provided the solid

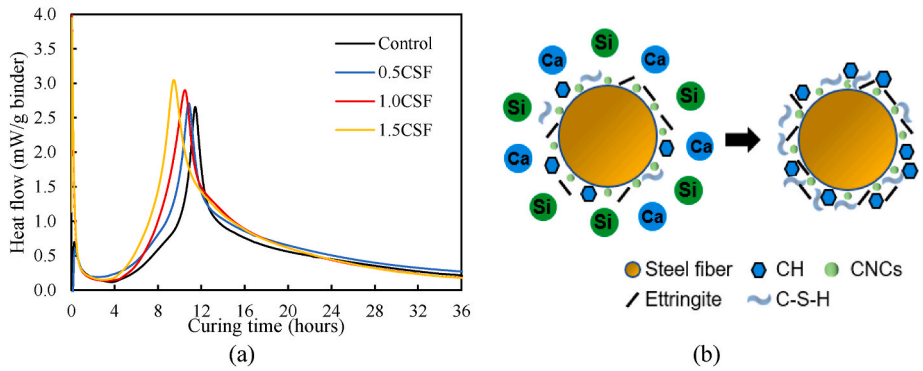

Fig. 15. Effect of CNCs coatings on hydration heat evolution of UHPC mixtures: (a) Results of hydration heat for UHPC with pristine and CNCs-coated steel fibers; (b) mechanism of CNCs.

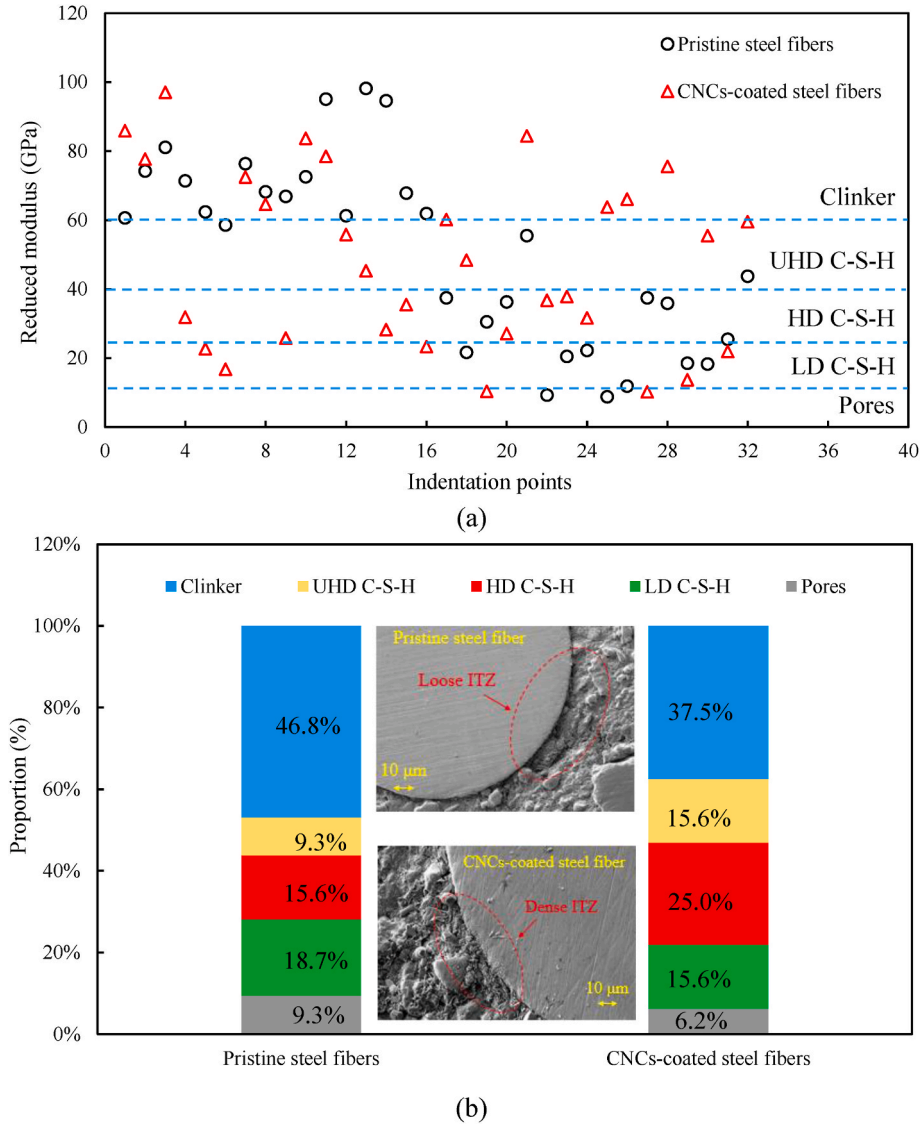

Fig. 16. Results of nanoindentation analysis: (a) schematic diagram of indentation points at the fiber-matrix interface; (b) SEM images of steel fibers embedded in UHPC matrix and phase proportions.

evidence that the coated CNCs film can densify the ITZ, which improved the bond strength on the interface and flexural performance of UHPC mixtures. This is attributed to the promoted cement hydration in the ITZ area validated in Section 4.2.5 [80,81,87].

5. Discussion

5.1. Flexural enhancement of UHPC with CNCs-coated steel fibers

5.1.1. Physical enhancement: increased surface roughness

The flexural enhancement of UHPC is clearly elaborated by the microstructural analysis on the surface of CNCs-coated steel fibers. Firstly, the surface morphology of the pristine and CNCs-coated steel fiber was characterized by SEM. Fig. 17(a) shows the surface of the pristine steel fiber surface, which is smooth and clean. Fig. 17(b)–(c), and Fig. 17(d) show the surface of CNCs-coated steel fibers treated by different CNCs concentrations. Plenty of CNCs particles with the white color was clearly visible on the surface of steel fibers, and the coating film was uniformly distributed, confirming the successful CNCs coating on surface of steel fibers which is in agreement with previous studies [52,90,91]. The surface of the coated steel fiber is speculated to be rougher. The quantified results of the roughness variation of the pristine and CNCs coated steel fibers was quantitatively evaluated the AFM measurement.

Subsequently, the three-dimensional AFM images of pristine and coated steel fibers were presented in Fig. 18(a–d). As summarized in Fig. 18(e), the surface of the pristine steel fibers is relatively smooth, and

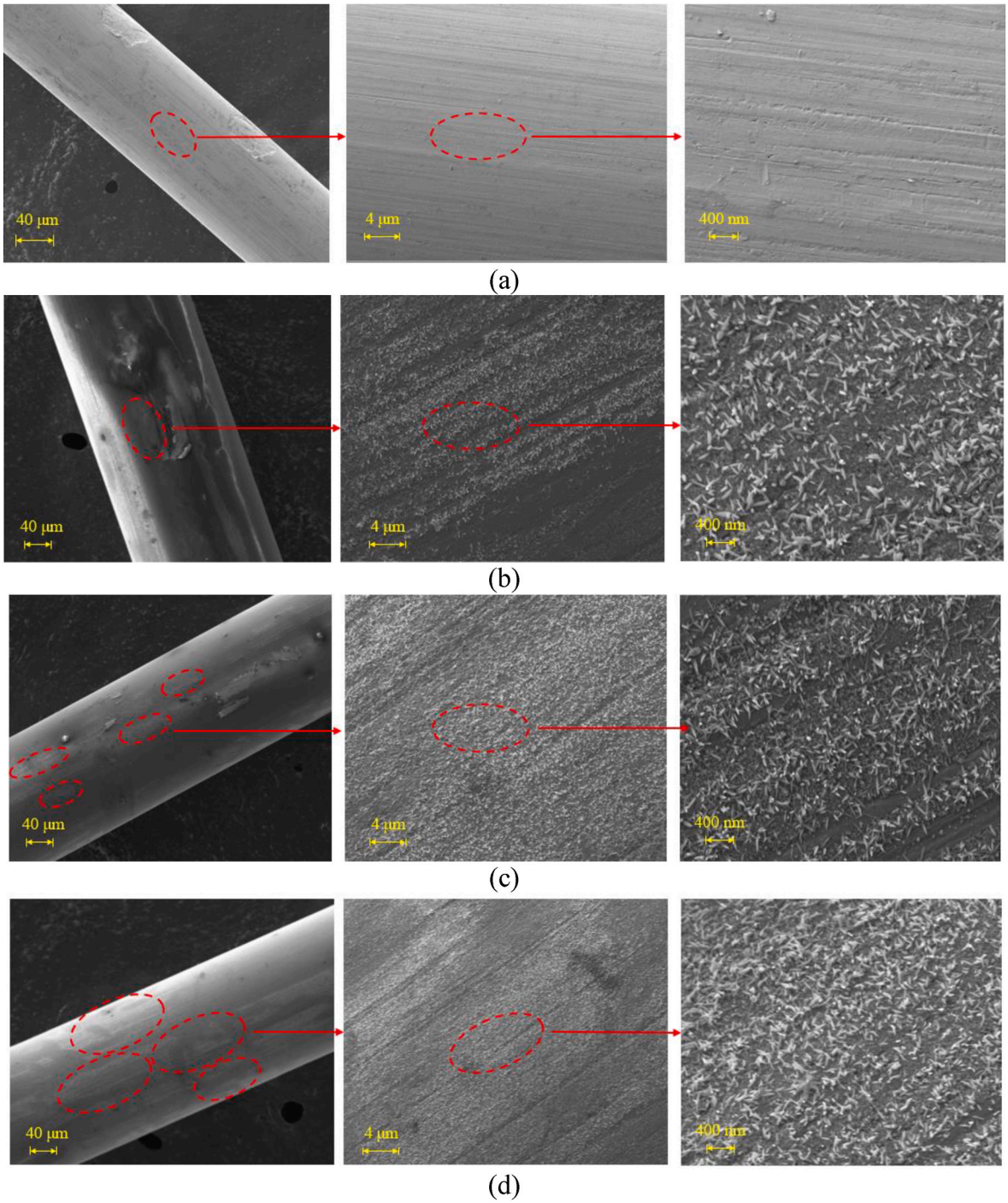

Fig. 17. Scanning electronic microscope (SEM) images of the: (a) pristine steel fiber; (b) coated steel fiber by 0.5 % CNC suspension (0.5CSF); (c) coated steel fiber by 1.0 % CNC suspension (1.0CSF); (c) coated steel fiber by 1.5 % CNC suspension (1.5CSF).

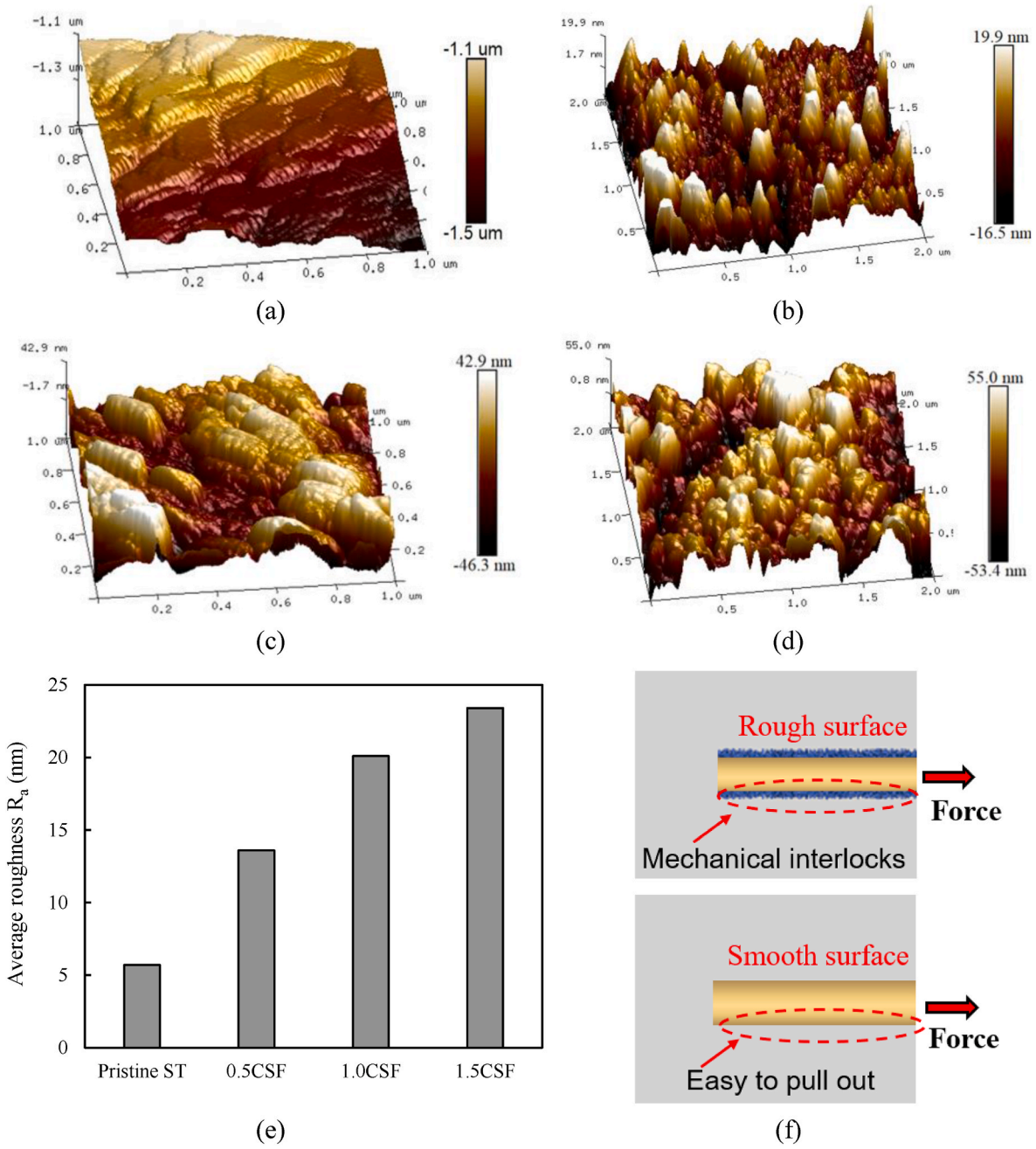

Fig. 18. Atomic force microscope (AFM) images of the: (a) pristine steel fiber; (b) coated steel fiber by 0.5 % CNC suspension (0.5CSF); (c) coated steel fiber by 1.0 % CNC suspension (1.0CSF); (c) coated steel fiber by 1.5 % CNC suspension (1.5CSF); (e) summarized results of the average roughness (R_a); (f) mechanism of physical enhancement by CNCs coatings on steel fibers.

the average roughness (i.e., R_a) is 5.7 nm. After the CNCs coating process, the average roughness value was increased to 20.1 nm by 255 %, indicating the significant increase of the surface roughness of the coated steel fibers. As elucidated in Fig. 17(f), the increased surface roughness on the surface of steel fibers enhances the mechanical interlocks between reinforced steel fibers and UHPC matrix, thus physically increasing the flexural performance of UHPC, which is in agreement with previous studies [42–44].

5.1.2. Chemical enhancement: improved reactivity and hydrophilicity

Beside the physical enhancement on the surface, the chemical elements on the pristine and CNCs-coated steel fiber surface were characterized by EDS spectrum and FTIR spectroscopy, as recommended in previous research [28]. **In Fig. 19(a),** Cu, Fe, C, and very limited O were detected by EDS on the surface of pristine steel fibers. After the CNCs suspension coating process, the steel fibers were covered with a thin film of CNCs particles as introduced before. Besides, the EDS spectrums in Fig. 19(b)–(c), and Fig. 19(d) indicate that the O content significantly increased from 8.17 % to 31.45 % after the CNCs suspension coating process. It is speculated the increasing O content is provided by the hydroxyl groups from CNCs particles. The origin of the O content on the surface of CNCs-coated steel fibers was validated by the FTIR test show below.

In addition, the functional groups on the CNCs-coated steel fiber surface were revealed by FTIR test, shown in Fig. 20. Similar peaks with wavenumbers of 1059 cm^{-1}, 1371 cm^{-1}, 1637 cm^{-1}, 2900 cm^{-1}, and 3406 cm^{-1} were observed in both CNCs particles and CNCs-coated steel fibers. Specifically, peaks at 1059 cm^{-1}, 1371 cm^{-1}, 1637 cm^{-1}, 2900

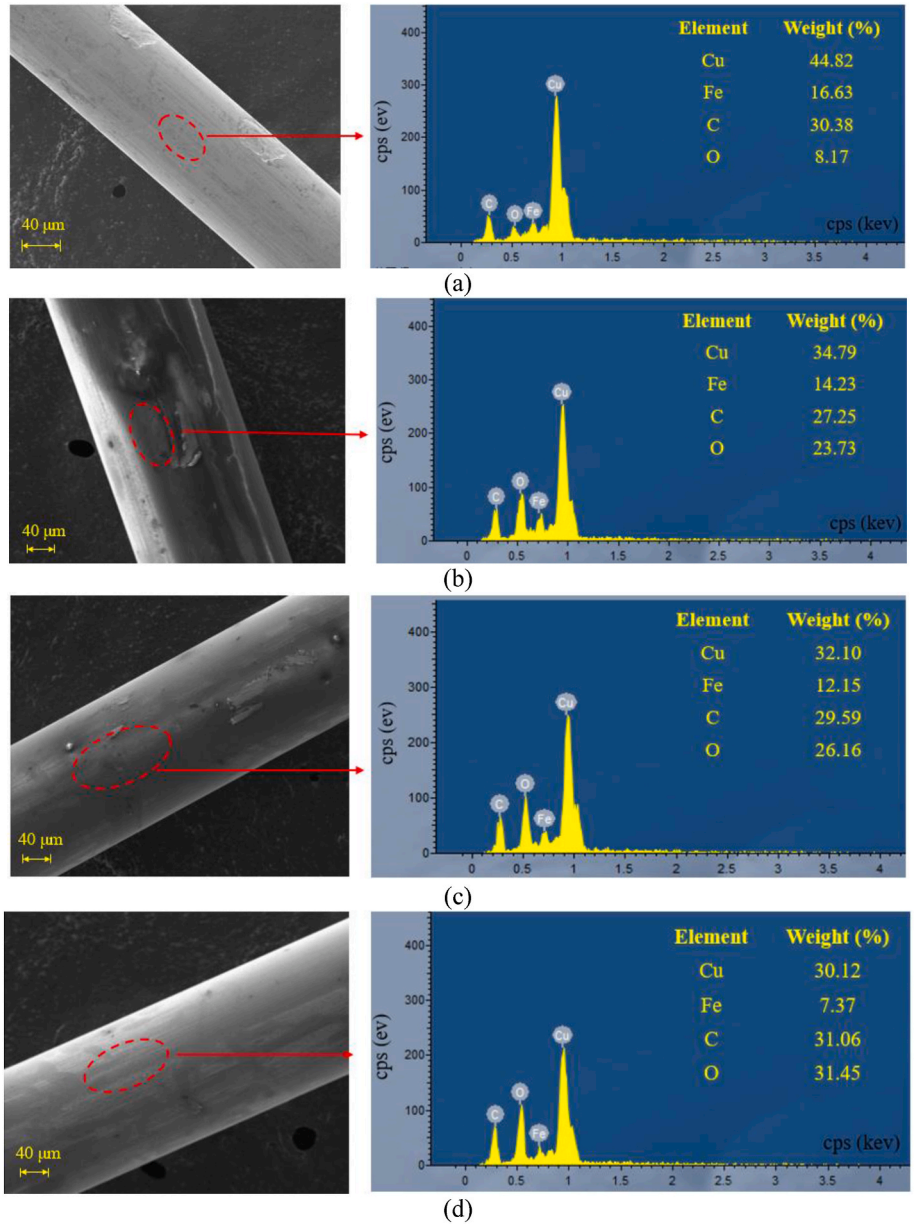

Fig. 19. Energy dispersive spectrometer (EDS) images of the: (a) pristine steel fiber; (b) coated steel fiber by 0.5 % CNC suspension (0.5CSF); (c) coated steel fiber by 1.0 % CNC suspension (1.0CSF); (d) coated steel fiber by 1.5 % CNC suspension (1.5CSF).

cm^{-1}, and 3406 cm^{-1} were attributed to the stretching vibration of C-O, C-H, absorbed water, and O-H functional groups, respectively. These functional groups were the major components in CNCs particles instead of pristine steel fibers. Therefore, these observations confirmed that the O content from the CNCs-coated steel fibers is from the CNCs particles and the CNCs film was successfully coated on the steel fiber surface [69, 70]. Moreover, the it helps promote the hydration of the UHPC matrix, shown in Section 4.2.5, and densifies the ITZ between steel fibers and UHPC matrix, shown in Section 4.2.6.

To the end, for the pristine steel fibers (i.e., brass-coated), the main surface composition is copper (Cu) which has poor hydrophilicity. The hydrophobic surface of pristine steel fiber results in inferior adhesion to UHPC matrix, thereby leading to easy debonding during fiber pullout process [30]. Therefore, the improvement of wettability on steel fiber surface can affect the performance of the ITZ. Fig. 21(a–d) shows the results of the contact angle between distilled water and pristine and CNCs-coated steel fibers. In general, the smaller contact angle represents the better wettability [92]. As summarized in Fig. 21(e), compared to the pristine steel fibers, the average contact angle of CNCs-coated steel fibers (i.e., 1.5CSF) was reduced from 71.9° to 51.2° by 28 %. The underlying mechanism is that the CNCs coating layer contains large amounts of hydroxyl groups (-OH), which increases the fiber polarity and reduces the fiber surface energy. Hence, the wettability of the CNCs-coated steel fibers was improved. Based on that, more free water is prone to transport to the ITZ area to the steel fiber surface to react with unhydrated cement particles, thus promoting the hydration reaction of UHPC validated in Section 4.2.5 and densifying the ITZ area validated in Section 4.2.6. Hence, the CNCs coatings chemically increases the flexural performance of UHPC, which is also in agreement with previous findings [93].

As shown in Fig. 22, the CNCs coating films on the surface of steel fibers act as a “double-sided tape” between steel fiber and UHPC matrix [51]. The CNCs coating films adhere to the steel fiber by the hydrogen bond, which increases the roughness of the steel fiber surface, thus increasing the physical interlocks. In addition, the CNCs coating films adhere to the UHPC matrix by short circuit diffusion effect, which

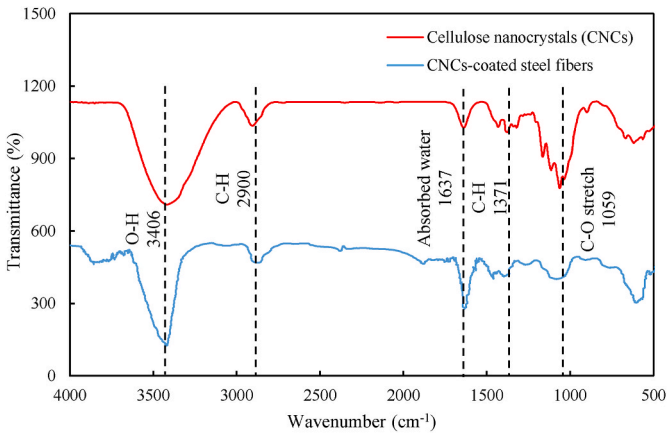

Fig. 20. FTIR spectra of cellulose nanocrystals (CNCs) and CNCs-coated steel fibers.

transport the free water from the capillary pores to the ITZ areas to react with the unhydrated cement particles, thus increasing the chemical bonding [81]. The coupled effect of physical and chemical enhancement can endow the densified ITZ between steel fibers and UHPC matrix. The findings can provide an in-depth understanding of microscale enhancement mechanisms of CNCs coating modification, contributing to a novel and effective approach for improving interfacial bond and flexural performance in UHPC.

The nano modification of steel fibers with cellulose nanocrystal (CNC) coatings significantly enhances the ITZ between the matrix and steel fibers, thereby improving the flexural performance of UHPC. This improvement can be attributed to the nano-core effect of the nano-materials, specifically the cellulose nanocrystals used in this study [94, 95]. On one hand, the small size of the nano-scale CNC particles allows them to fill the pores and densify the ITZ, a phenomenon referred to as the nano effect [96]. On the other hand, the high specific surface area and surface energy of the CNC particles result in a nucleating effect that facilitates the hydration of cementitious materials, which is referred to the core effect [97]. In summary, the combination of the nano effect and core effect, termed the nano-core effect, provides a comprehensive explanation for the enhanced flexural performance of UHPC reinforced with CNC-coated steel fibers.

5.2. Flexural reduction of UHPC with CNCs-coated steel fibers

5.2.1. Contradiction between increased bond strength and reduced flexural strength

As shown in the single fiber pull-out test (Section 4.2.4) and ITZ characterization (Section 4.2.6), when a higher concentration of CNCs suspension was used to modify pristine steel fibers, it is possible to achieve a higher bond strength and a denser interface for the steel fibers and UHPC matrix. However, both the results of compressive tests and flexural tests showed the lower mechanical strengths and lower toughness were reached when the concentration of CNCs coating suspension exceeds the threshold value (i.e., 1.0 %). It is speculated that, while the higher concentration of CNCs coating suspension improves the interface between UHPC matrix and steel fiber, the high concentration (especially

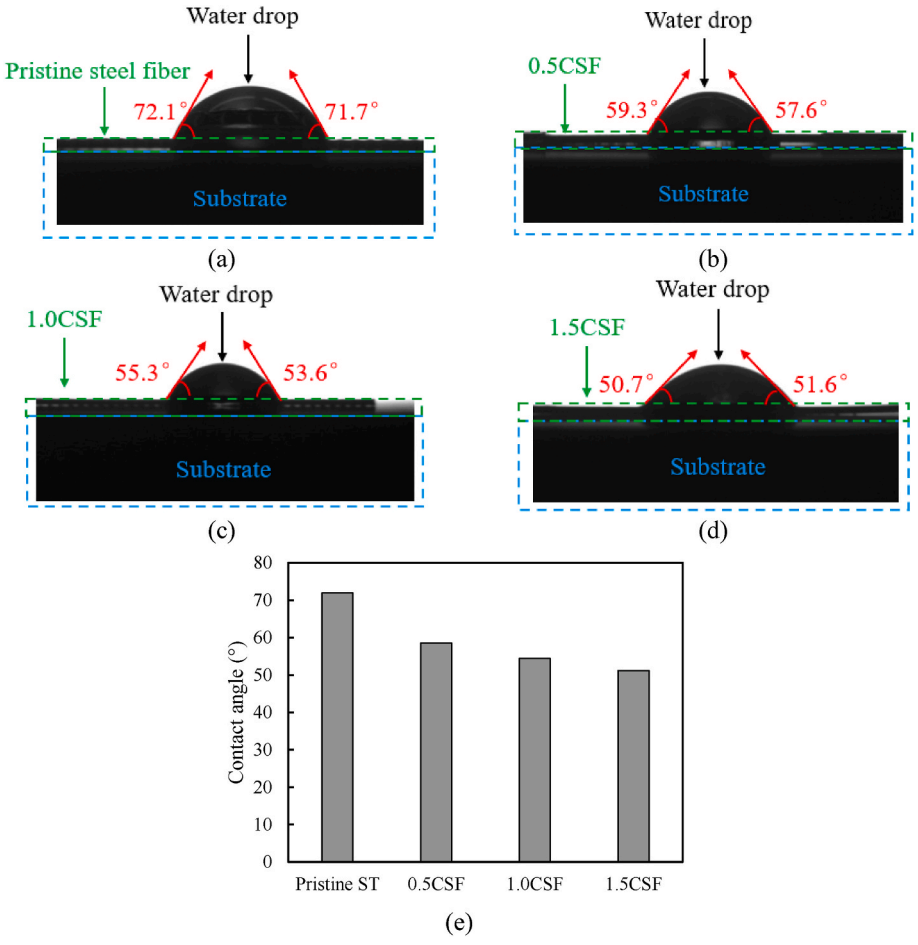

Fig. 21. Contact angle measurements of the: (a) pristine steel fiber; (b) coated steel fiber by 0.5 % CNC suspension (0.5CSF); (c) coated steel fiber by 1.0 % CNC suspension (1.0CSF); (c) coated steel fiber by 1.5 % CNC suspension (1.5CSF); (e) summarized results of the contact angle.

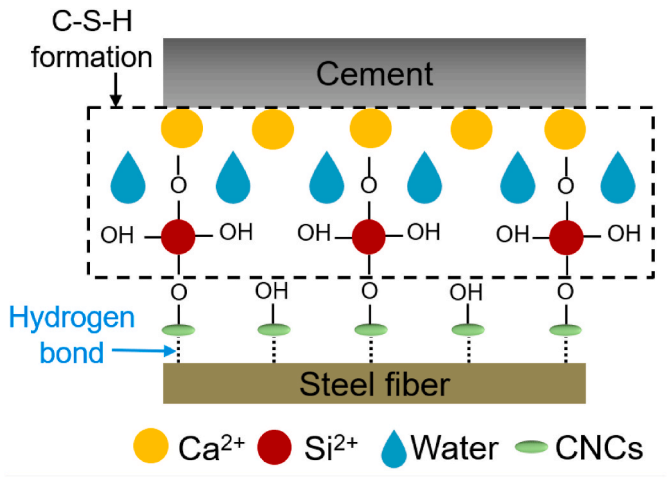

Fig. 22. Underlying mechanism of CNCs on surface of steel fibers on performance of UHPC.

over the threshold value) is prone to cause gelation of CNCs suspension after the coating process. In the nutshell, the CNCs coating film would stick the uniformly dispersed steel fibers together, seriously affecting its distribution.

5.2.2. Reduced fiber dispersion and orientation

After the flexural test for the UHPC with pristine and CNCs-coated steel fibers, four slices with 76 × 76 × 10 mm were cut from the one side of the major crack of the UHPC beams. The cutting planes were parallel to the cross section of UHPC beams. The image processing technique was adopted from the previous research [98] to quantitatively evaluate the fiber dispersion (α) and orientation (η) in the UHPC matrix, based on the coordinates of fibers and the shape of the fibers in the cutting plane.

Firstly, The RGB images were converted into binary images using the software (i.e., Image J) [99], which enables the fibers to be distinguished from the surrounding matrix according to the brightness. The 76 × 76 mm image corresponding to the total cross-sectional area was divided into 21 × 21 units. Then, the number of fibers per unit was counted. The uniformity of fiber distribution of the whole cross section was quantified using a fiber dispersion coefficient (α). This coefficient expresses the deviation of the number of fibers in a unit area from the average number of fibers, as expressed by Eq. (5) [32,33]:

$$\alpha = \exp\left[-\frac{1}{x_0}\sqrt{\frac{\sum (x_i - x_0)^2}{n}}\right] \tag{5}$$

where n represents the number of the units, x_i represents the number of fibers in the i-th unit, and x_0 represents the average number of fibers in each unit. The α value approaches to 1 for uniformly-dispersed fibers in the matrix, or 0 for a severely-biased dispersion.

Fig. 23 shows the geometry of an inclined fiber and the section in the cutting plane, The major axis length (L) and the diameter (D) of each fiber were measured by specifying the lengths (in pixels) of the major and minor axes of the ellipse. High-resolution images were employed to prevent false detection of fiber orientation [100]. In this study, the resolution was 60 pixels, in order to accommodate the 0.2-mm diameter of the steel fibers.

The fiber orientation was defined as the angle between the fiber axis and the normal direction which is perpendicular to the cutting plane, as shown in Eqs. (6) and (7). In order to evaluate the effect of fiber orientation on flexural properties of UHPC, a fiber orientation coefficient (η) was introduced, considering the probability density distribution of the fiber orientation [101]:

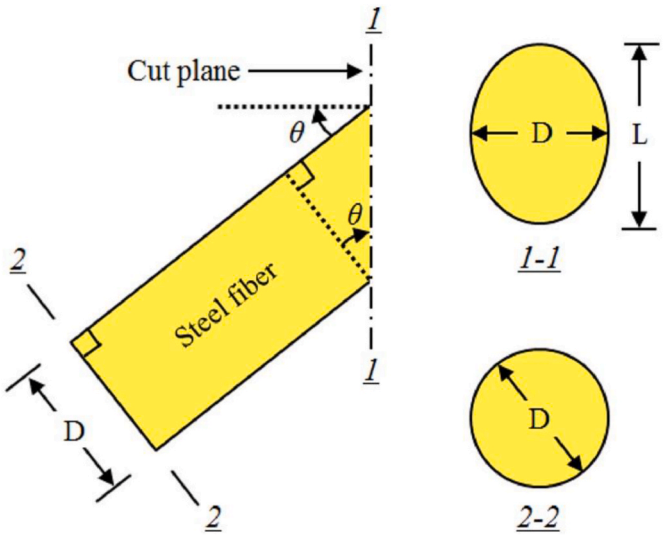

Fig. 23. Example of an inclined steel fiber in UHPC matrix. Where θ, D, and L correspond to the inclined angle ($0 \le \theta \le \pi/2$), diameter of the fiber, and the major axis length of the fiber image.

$$\theta = \arccos\left(\frac{D}{L}\right) \tag{6}$$

$$\eta = \int_{\theta_{min}}^{\theta_{max}} p(\theta)\cos^2\theta d\theta \tag{7}$$

Where, when η approaches to 1, all the fibers are aligned perpendicular to the cross section, and when η equals to 0, all the fibers are aligned parallel to the cross section. p(θ) represents the probability density distribution for the fiber orientation.

Fig. 24 shows the RGB and binary cutting images of the control, 0.5CSF, 1.0CSF, and 1.5CSF, respectively. In general, the steel fibers are uniformly dispersed in the cubic section, shown in Fig. 24(a–c), which can be attributed to the proper viscosity of UHPC mortar and initially well-dispersed steel fibers. By contrast, more steel fibers are observed at one side of the cubic section, shown in Fig. 24(d), indicating the fiber segregation. Considering that the UHPC mortar is the same for all investigated UHPC mixtures, the CNCs-coated steel fibers (1.5CSF) should be responsible for the poor distribution.

Fig. 25(a) plots the values of fiber dispersion (α) and fiber orientation (η), which are determined by image analysis [98]. Results showed that, compared to the control mixture, the α and η of 1.5CSF were decreased from 0.64 to 0.59 (by 8 %) and from 0.52 to 0.25 (by 50 %), indicating the significant reduction in the fiber distribution. In addition, the serious agglomeration picture of steel fibers after the CNCs coating process (in 1.5CSF mixture) was also shown in Fig. 25(b). As the reduction of both fiber dispersion and orientation in UHPC mixture, the flexural performance was negatively affected, shown in Fig. 25(c–d). Therefore, the fiber distribution analysis suggested that steel fibers treated by a high concentration of CNCs suspension are prone to agglomeration, which leads to a performance reduction.

6. Conclusions

This research aims to provide a sustainable method to densify the ITZ by coating CNCs particles on surface of steel fibers, and then enhance the flexural performance of UHPC mixtures. Comprehensive experiments were conducted to evaluate the CNCs coating suspensions, CNCs-coated steel fibers, and UHPC with CNCs-coated steel fibers, respectively. The optimal concentration of CNCs coating suspension was determined. Moreover, the underlying mechanisms of the effect of CNCs-coated steel

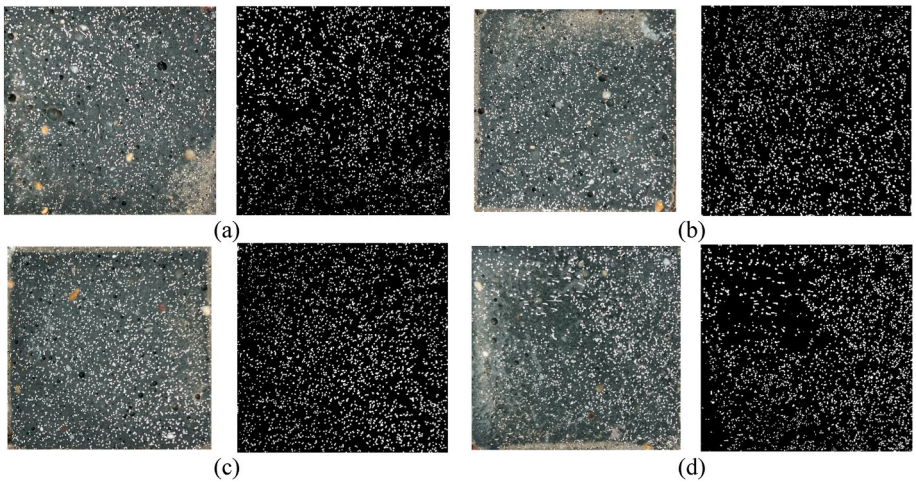

Fig. 24. Cutting plane image of UHPC mixtures with pristine and CNCs-coated steel fibers: (a) RGB and binary images of control; (b) RGB and binary images of 0.5CSF; (c) RGB and binary images of 1.0CSF; (d) RGB and binary images of 1.5CSF.

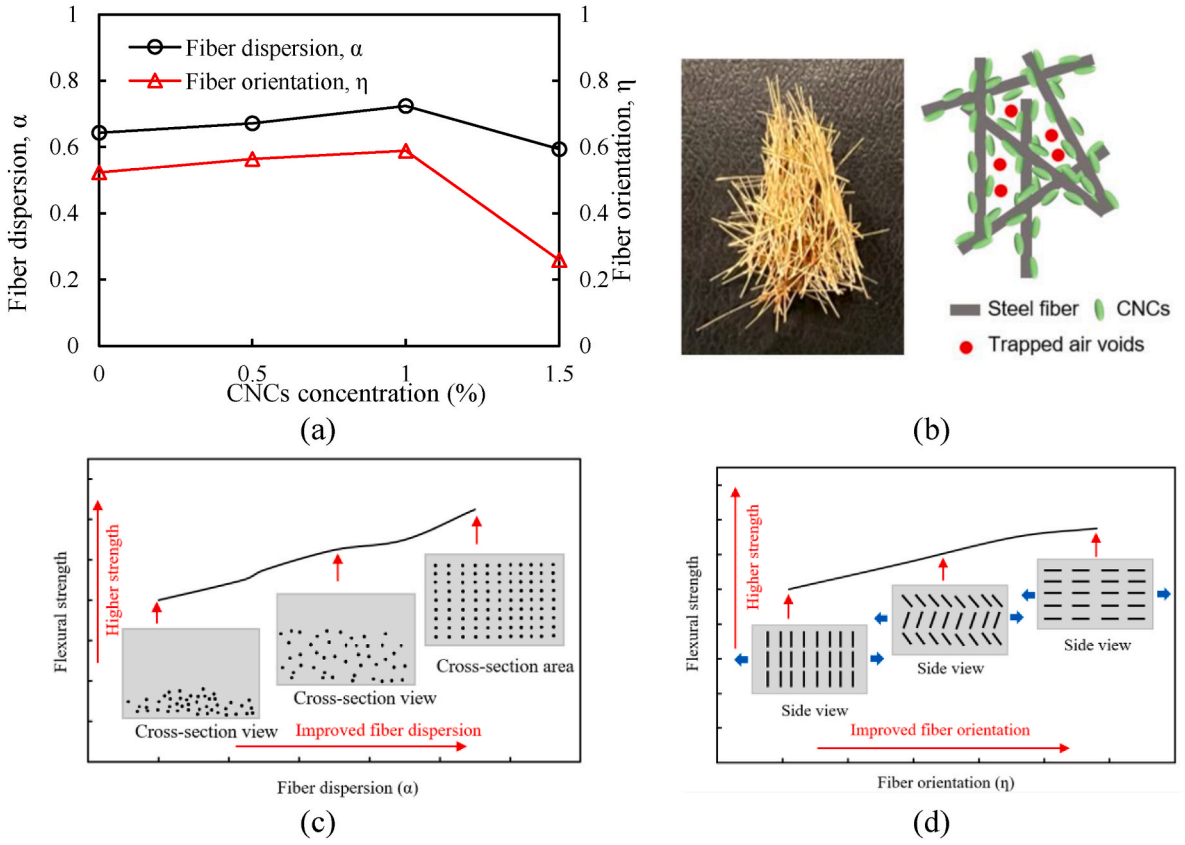

Fig. 25. Results of fiber dispersion and orientation coefficients in UHPC mixtures.

fibers on different properties of UHPC were discussed. Based on the above investigations, the following conclusion are drawn.

(1) The flow index of CNCs coating suspension based on the Herschel-Bulkley model were investigated to determine the critical CNCs concentration (i.e., 1.0 %). Over the critical concentration, the CNCs coating film would stick the uniformly dispersed steel fibers together and then affect their distribution, thus reducing the mechanical performance of UHPC.
(2) The macroscale mechanical properties of UHPC with CNCs-coated and pristine steel fibers were comprehensively investigated. Results showed that, when pristine steel fibers are coated by the optimal CNCs suspension (i.e., 1.0CSF), the compressive strength, flexural strength, and toughness of UHPC were increased by 5 %, 14 %, and 18 %, respectively.
(3) The single fiber pull-out test and ITZ characterization indicated that the CNCs film significantly increased the bond strength and pull-out energy by 13 % and 50 % to densify the interface between UHPC matrix and steel fibers, thus improving the mechanical performance of UHPC.
(4) The microscale characterization on modified and pristine steel fibers indicated that the CNCs film was successfully coated on the

surface of steel fibers. Specifically, the average roughness of CNCs-coated steel fibers increased from 5.7 mm to 20.1 mm by 255 %, resulting in higher mechanical interlock. Besides, the oxygen content was increased from 8.17 % to 31.45 % after the CNCs suspension coating process which is from the reactive functional groups (e.g., -OH), enhancing the reactivity. Finally, the average contact angle of CNCs-coated steel fibers (i.e., 1.5CSF) was reduced from 71.9° to 51.2°, validating the improved hydrophilicity. The molecular simulation will be further conducted on the ITZ between UHPC matrix and steel fibers to help understand the effect of CNCs coatings from the theoretical aspects.

(5) The key limitation is, due to the severe agglomeration of CNCs suspension under high concentrations, the CNCs' coating efficiency is relatively limited. Further research is needed to achieve the well dispersion of CNCs particles in tap water under higher concentrations, thus further enhancing the flexural properties of UHPC.

CRediT authorship contribution statement

Jiang Du: Writing – original draft, Visualization, Investigation, Formal analysis, Data curation. **Yuhuan Wang:** Writing – review & editing, Investigation, Data curation. **Pengwei Guo:** Writing – review & editing, Methodology, Data curation. **Weina Meng:** Writing – review & editing, Supervision, Resources, Project administration, Funding acquisition, Conceptualization.

Declaration of competing interest

The authors declare that they have no known competing financial interests or personal relationships that could have appeared to influence the work reported in this paper.

Data availability

Data will be made available on request.

Acknowledgement

This research is supported by the National Science Foundation [grant number CMMI-2046407]. The authors also would like to thank Lehigh Hanson for the donation of Type I cement and GGBFS.

References

[1] C. Shi, Z. Wu, J. Xiao, D. Wang, Z. Huang, Z. Fang, A review on ultra high performance concrete: Part I. Raw materials and mixture design, Construct. Build. Mater. 101 (2015) 741–751.
[2] 239, A.C. *Ultra-high-performance Concrete: an Emerging Technology Report (ACI 239R-18)*, American Concrete Institute, 2018.
[3] Y. Kusumawardaningsih, E. Fehling, M. Ismail, A.A.M. Aboubakr, Tensile strength behavior of UHPC and UHPFRC, Procedia Eng. 125 (2015) 1081–1086.
[4] T. Alahmari, C. Kennedy, A. Cuaron, B. Weldon, D. Jauregui, Field testing of a prestressed concrete bridge with high performance and locally developed ultra-high performance girders, Frontiers in Built Environment 5 (2019) 114.
[5] S. Aaleti, S. Sritharan, A. Abu-Hawash, Innovative UHPC-normal concrete composite bridge deck, in: F. Toutlemonde, J. Resplendino (Eds.), Proceedings of the RILEM-Fib-AFGC International Symposium on Ultra-high Performance Reinforced Concrete, Rilem Publications SARL, Bagneux, France, 2013.
[6] T.V. Voort, M.T. Suleiman, S. Sritharan, Design and Performance Verification of Ultra-high Performance Concrete Piles for Deep Foundations, Iowa State University. Center for Transportation Research and Education, 2008.
[7] J. Qi, Y. Bao, J. Wang, L. Li, W. Li, Flexural behavior of an innovative dovetail UHPC joint in composite bridges under negative bending moment, Eng. Struct. 200 (2019) 109716.
[8] B. Graybeal, Field-cast UHPC Connections for Modular Bridge Deck Elements, 2010.
[9] B.A. Graybeal, Ultra-high Performance Concrete Composite Connections for Precast Concrete Bridge Decks, Federal Highway Administration. Office of Infrastructure Research and Development, United States, 2012.
[10] S. Verger-Leboeuf, J.-P. Charron, B. Massicotte, Design and behavior of UHPFRC field-cast transverse connections between precast bridge deck elements, J. Bridge Eng. 22 (7) (2017) 04017031.
[11] J. Leng, J. Yang, Z. Zhang, J. Du, Y. Zou, J. Zhou, Effect of vehicle-induced vibration on the strength, nano-mechanical properties, and microstructural characteristics of ultra-high-performance concrete during hardening process, Cement Concr. Compos. 148 (2024) 105487.
[12] J. Leng, J. Yang, Z. Zhang, Y. Zou, J. Du, J. Zhou, Mechanical behavior of a novel compact steel-UHPC joint for hybrid girder bridges: experimental and numerical investigation, Journal of Constructional Steel Research 218 (2024) 108742.
[13] J. Xie, Q. Fu, J.-B. Yan, Compressive behaviour of stub concrete column strengthened with ultra-high performance concrete jacket, Construct. Build. Mater. 204 (2019) 643–658.
[14] H. Zhang, X. Ma, H. Jiang, K. Tong, Y. Zheng, J. Zhou, Grading evaluation of overall corrosion degree of corroded RC beams via SMFL technique, Struct. Control Health Monit. 2023 (2023).
[15] Z.B. Haber, J.F. Munoz, B.A. Graybeal, Field Testing of an Ultra-high Performance Concrete Overlay, Federal Highway Administration. Office of Infrastructure …, United States, 2017.
[16] K.H. Khayat, M. Valipour, Design of Ultra High Performance Concrete as an Overlay in Pavements and Bridge Decks, Missouri University of Science and Technology. Center for Transportation Infrastructure and Safety, 2014.
[17] Z.B. Haber, J.F. Munoz, I. De la Varga, B.A. Graybeal, Bond characterization of UHPC overlays for concrete bridge decks: laboratory and field testing, Construct. Build. Mater. 190 (2018) 1056–1068.
[18] H. Wibowo, S. Sritharan, Use of Ultra-high-performance Concrete for Bridge Deck Overlays, Federal Highway Administration, United States, 2018.
[19] L. Teng, M. Valipour, K.H. Khayat, Design and performance of low shrinkage UHPC for thin bonded bridge deck overlay, Cement Concr. Compos. (2021) 103953.
[20] J. Du, P. Guo, Z. Liu, W. Meng, Highly thixotropic ultra-high-performance concrete (UHPC) as an overlay, Construct. Build. Mater. 366 (2023) 130130.
[21] Y. Zou, K. Zheng, Z. Zhou, Z. Zhang, J. Guo, J. Jiang, Experimental study on flexural behavior of hollow steel-UHPC composite bridge deck, Eng. Struct. 274 (2023) 115087.
[22] P. Guo, W. Meng, J. Du, L. Stevenson, B. Han, Y. Bao, Lightweight ultra-high-performance concrete (UHPC) with expanded glass aggregate: development, characterization, and life-cycle assessment, Construct. Build. Mater. 371 (2023) 130441.
[23] R. Chen, Z. Zhang, Y. Zou, J. Yang, J. Zhou, Y. Kuang, Y. Wang, In-situ evaluation on existing RC beam strengthened with GFRP-reinforced UHPC overlay, Construct. Build. Mater. 429 (2024) 136363.
[24] J. Yang, R. Chen, Z. Zhang, Y. Zou, J. Zhou, J. Xia, Experimental study on the ultimate bearing capacity of damaged RC arches strengthened with ultra-high performance concrete, Eng. Struct. 279 (2023) 115611.
[25] J. Yang, J. Xia, Z. Zhang, Y. Zou, Z. Wang, J. Zhou, Experimental and numerical investigations on the mechanical behavior of reinforced concrete arches strengthened with UHPC subjected to asymmetric load, in: Structures, Elsevier, 2022.
[26] Y. Zou, J. Jiang, J. Yang, Z. Zhang, J. Guo, Enhancing the toughness of bonding interface in steel-UHPC composite structure through fiber bridging, Cement Concr. Compos. 137 (2023) 104947.
[27] J.-Y. Wang, J.-Y. Guo, Damage investigation of ultra high performance concrete under direct tensile test using acoustic emission techniques, Cement Concr. Compos. 88 (2018) 17–28.
[28] T. Liu, H. Wei, A. Zhou, D. Zou, H. Jian, Multiscale investigation on tensile properties of ultra-high performance concrete with silane coupling agent modified steel fibers, Cement Concr. Compos. 111 (2020) 103638.
[29] H. Zhang, J. Qi, Y. Zheng, J. Zhou, J. Qiu, Characterization and grading assessment of rebar corrosion in loaded RC beams via SMFL technology, Construct. Build. Mater. 411 (2024) 134484.
[30] A. Zhou, H. Wei, T. Liu, D. Zou, Y. Li, R. Qin, Interfacial technology for enhancement in steel fiber reinforced cementitious composite from nano to macroscale, Nanotechnol. Rev. 10 (1) (2021) 636–652.
[31] J. Du, W. Meng, K.H. Khayat, Y. Bao, P. Guo, Z. Lyu, A. Abu-obeidah, H. Nassif, H. Wang, New development of ultra-high-performance concrete (UHPC), Compos. B Eng. (2021) 109220.
[32] L. Teng, W. Meng, K.H. Khayat, Rheology control of ultra-high-performance concrete made with different fiber contents, Cement Concr. Res. 138 (2020) 106222.
[33] H. Huang, X. Gao, L. Teng, Fiber alignment and its effect on mechanical properties of UHPC: an overview, Construct. Build. Mater. 296 (2021) 123741.
[34] Z. Zhang, K. Pang, L. Xu, Y. Zou, J. Yang, C. Wang, The bond properties between UHPC and stone under different interface treatment methods, Construct. Build. Mater. 365 (2023) 130092.
[35] Y. Zou, K. Yu, J. Heng, Z. Zhang, H. Peng, C. Wu, X. Wang, Feasibility study of new GFRP grid web-Concrete composite beam, Compos. Struct. 305 (2023) 116527.
[36] K. Yue, L. Xu, J. Liu, L. Fan, L. Xu, Seismic performance of an energy dissipating shear key for highway bridges using butterfly-shaped steel plates, Eng. Struct. 295 (2023) 116885.
[37] Z. Wu, C. Shi, K.H. Khayat, Investigation of mechanical properties and shrinkage of ultra-high performance concrete: influence of steel fiber content and shape, Compos. B Eng. 174 (2019) 107021.

[38] W. Meng, K.H. Khayat, Effect of hybrid fibers on fresh properties, mechanical properties, and autogenous shrinkage of cost-effective UHPC, J. Mater. Civ. Eng. 30 (4) (2018) 04018030.
[39] P. Shen, L. Lu, Y. He, F. Wang, S. Hu, The effect of curing regimes on the mechanical properties, nano-mechanical properties and microstructure of ultra-high performance concrete, Cement Concr. Res. 118 (2019) 1–13.
[40] W. Li, Z. Huang, F. Cao, Z. Sun, S.P. Shah, Effects of nano-silica and nano-limestone on flowability and mechanical properties of ultra-high-performance concrete matrix, Construct. Build. Mater. 95 (2015) 366–374.
[41] H.D. Miller, A. Akbarnezhad, S. Mesgari, S.J. Foster, Performance of oxygen/argon plasma-treated steel fibres in cement mortar, Cement Concr. Compos. 97 (2019) 24–32.
[42] D. Aggelis, D. Soulioti, N. Barkoula, A. Paipetis, T. Matikas, Influence of fiber chemical coating on the acoustic emission behavior of steel fiber reinforced concrete, Cement Concr. Compos. 34 (1) (2012) 62–67.
[43] J. Du, W. Meng, K.H. Khayat, Y. Bao, P. Guo, Z. Lyu, A. Abu-Obeidah, H. Nassif, H. Wang, New development of ultra-high-performance concrete (UHPC), Compos. B Eng. 224 (2021) 109220.
[44] Y. Deng, Z. Zhang, C. Shi, Z. Wu, C. Zhang, Steel fiber–matrix interfacial bond in ultra-high performance concrete: a review, Engineering 22 (2023) 215–232.
[45] D.-Y. Yoo, S. Kim, G.-J. Park, J.-J. Park, S.-W. Kim, Effects of fiber shape, aspect ratio, and volume fraction on flexural behavior of ultra-high-performance fiber-reinforced cement composites, Compos. Struct. 174 (2017) 375–388.
[46] Z. Liu, J. Du, W. Meng, Achieving low-carbon cementitious materials with high mechanical properties using CaCO3 suspension produced by CO2 sequestration, J. Clean. Prod. 373 (2022) 133546.
[47] W. Meng, K.H. Khayat, Effect of graphite nanoplatelets and carbon nanofibers on rheology, hydration, shrinkage, mechanical properties, and microstructure of UHPC, Cement Concr. Res. 105 (2018) 64–71.
[48] N.T. Tran, D.J. Kim, Synergistic response of blending fibers in ultra-high-performance concrete under high rate tensile loads, Cement Concr. Compos. 78 (2017) 132–145.
[49] J. Du, Z. Liu, C. Christodoulatos, M. Conway, Y. Bao, W. Meng, Utilization of off-specification fly ash in preparing ultra-high-performance concrete (UHPC): mixture design, characterization, and life-cycle assessment, Resour. Conserv. Recycl. 180 (2022) 106136.
[50] A. Radhamani, H.C. Lau, S. Ramakrishna, CNT-reinforced metal and steel nanocomposites: a comprehensive assessment of progress and future directions, Compos. Appl. Sci. Manuf. 114 (2018) 170–187.
[51] Z. Pi, H. Xiao, R. Liu, M. Liu, H. Li, Effects of brass coating and nano-SiO2 coating on steel fiber–matrix interfacial properties of cement-based composite, Compos. B Eng. 189 (2020) 107904.
[52] D.-Y. Yoo, N. Banthia, Y.-S. Yoon, Recent development of innovative steel fibers for ultra-high-performance concrete (UHPC): a critical review, Cement Concr. Compos. 145 (2024) 105359.
[53] T. Stengel, Effect of surface roughness on the steel fibre bonding in ultra high performance concrete (UHPC), in: Nanotechnology in Construction 3, Springer Berlin Heidelberg, Berlin, Heidelberg, 2009.
[54] B. Chun, D.-Y. Yoo, N. Banthia, Achieving slip-hardening behavior of sanded straight steel fibers in ultra-high-performance concrete, Cement Concr. Compos. 113 (2020) 103669.
[55] D.-Y. Yoo, Y.S. Jang, T. Oh, N. Banthia, Use of engineered steel fibers as reinforcements in ultra-high-performance concrete considering corrosion effect, Cement Concr. Compos. 133 (2022) 104692.
[56] Y.S. Jang, D.-Y. Yoo, Combined chelating and corrosion effects of steel fiber on the interfacial bond and tensile behaviors of ultra-high-performance concrete, Cement Concr. Compos. 129 (2022) 104505.
[57] S. Kim, S. Choi, D.-Y. Yoo, Surface modification of steel fibers using chemical solutions and their pullout behaviors from ultra-high-performance concrete, J. Build. Eng. 32 (2020) 101709.
[58] T. Sugama, N. Carciello, L.E. Kukacka, G. Gray, Interface between zinc phosphate-deposited steel fibres and cement paste, J. Mater. Sci. 27 (11) (1992) 2863–2872.
[59] Y. Zhu, Y. Zhang, S. Qu, A. Kumar, Flexural and tensile strength of ultra-high-performance concrete with ZnPh-treated steel fibers, J. Mater. Civ. Eng. 32 (10) (2020) 06020013.
[60] Z. Pi, H. Xiao, J. Du, M. Liu, H. Li, Interfacial microstructure and bond strength of nano-SiO2-coated steel fibers in cement matrix, Cement Concr. Compos. 103 (2019) 1–10.
[61] A. Bashiri Rezaie, M. Liebscher, M. Ranjbarian, F. Simon, C. Zimmerer, A. Drechsler, R. Frenzel, A. Synytska, V. Mechtcherine, Enhancing the interfacial bonding between PE fibers and cementitious matrices through polydopamine surface modification, Compos. B Eng. 217 (2021) 108817.
[62] B. Chun, D.-Y. Yoo, N.J.C. Banthia, C. Composites, Achieving Slip-Hardening Behavior of Sanded Straight Steel Fibers in Ultra-high-performance Concrete, 113, 2020 103669.
[63] K. Yue, L. Xu, J. Liu, L. Fan, L. Xu, Energy dissipation evaluation of butterfly-shaped steel plate shear keys under different loading protocols, in: Structures, Elsevier, 2024.
[64] R.J. Moon, A. Martini, J. Nairn, J. Simonsen, J. Youngblood, Cellulose nanomaterials review: structure, properties and nanocomposites, Chem. Soc. Rev. 40 (7) (2011) 3941–3994.
[65] L. Brinchi, F. Cotana, E. Fortunati, J. Kenny, Production of nanocrystalline cellulose from lignocellulosic biomass: technology and applications, Carbohydr. Polym. 94 (1) (2013) 154–169.
[66] R. Reshmy, E. Philip, A. Madhavan, A. Pugazhendhi, R. Sindhu, R. Sirohi, M. K. Awasthi, A. Pandey, P. Binod, Nanocellulose as green material for remediation of hazardous heavy metal contaminants, J. Hazard Mater. 424 (2022) 127516.
[67] R.J. Moon, G.T. Schueneman, J. Simonsen, Overview of cellulose nanomaterials, their capabilities and applications, Jom 68 (9) (2016) 2383–2394.
[68] Y. Cao, P. Zavattieri, J. Youngblood, R. Moon, J. Weiss, The relationship between cellulose nanocrystal dispersion and strength, Construct. Build. Mater. 119 (2016) 71–79.
[69] J. Goswami, E. Haque, D.M. Fox, J.W. Gilman, G.A. Holmes, R.J. Moon, K. Kalaitzidou, The effect of cellulose nanocrystal coatings on the glass fiber–epoxy interphase, Materials 12 (12) (2019) 1951.
[70] A. Asadi, M. Miller, R. Moon, K. Kalaitzidou, Improving the interfacial and mechanical properties of short glass fiber/epoxy composites by coating the glass fibers with cellulose nanocrystals, Express Polym. Lett. 10 (7) (2016) 587–597, 10 (7): pp. 587–597.
[71] X.M. Dong, J.-F. Revol, D.G. Gray, Effect of microcrystallite preparation conditions on the formation of colloid crystals of cellulose, Cellulose 5 (1998) 19–32.
[72] D. Bondeson, I. Kvien, K. Oksman, Strategies for preparation of cellulose whiskers from microcrystalline cellulose as reinforcement in nanocomposites, in: Cellulose Nanocomposites, American Chemical Society, 2006, pp. 10–25.
[73] A. Zhou, Z. Yu, H. Wei, L.-h. Tam, T. Liu, D. Zou, Understanding the toughening mechanism of silane coupling agents in the interfacial bonding in steel fiber-reinforced cementitious composites, ACS Appl. Mater. Interfaces 12 (39) (2020) 44163–44171.
[74] Y. Chen, X. Zhou, X. Yin, Q. Lin, M. Zhu, A novel route to modify the interface of glass fiber-reinforced epoxy resin composite via bacterial cellulose, International Journal of Polymeric Materials and Polymeric Biomaterials 63 (4) (2014) 221–227.
[75] W. Meng, M. Valipour, K.H. Khayat, Optimization and performance of cost-effective ultra-high performance concrete, Materials and structures 50 (1) (2017) 29.
[76] J. Du, P. Guo, W. Meng, Effect of water-based nanoclay and ambient temperature on rheological properties of UHPC pastes, Construct. Build. Mater. 370 (2023) 130733.
[77] ASTM C230, Standard Specification for Flow Table for Use in Tests of Hydraulic Cement, ASTM International, 2021.
[78] ASTM C109/C109M-20b, Standard Test Method for Compressive Strength of Hydraulic Cement Mortars, ASTM International, 2020.
[79] ASTM C1609/C1609M-19a, Standard Test Method for Flexural Performance of Fiber-Reinforced Concrete, ASTM International, 2019.
[80] Y. Wang, S. Goodman, Y. Bao, W. Meng, Morphological, microstructural, and mechanical properties of highly-ordered C–S–H regulated by cellulose nanocrystals (CNCs), Cement Concr. Compos. 143 (2023) 105276.
[81] Y. Cao, P. Zavaterri, J. Youngblood, R. Moon, J. Weiss, The influence of cellulose nanocrystal additions on the performance of cement paste, Cement Concr. Compos. 56 (2015) 73–83.
[82] L. Lewis, M. Derakhshandeh, S.G. Hatzikiriakos, W.Y. Hamad, M.J. MacLachlan, Hydrothermal gelation of aqueous cellulose nanocrystal suspensions, Biomacromolecules 17 (8) (2016) 2747–2754.
[83] S. Förster, M. Konrad, P. Lindner, Shear thinning and orientational ordering of wormlike micelles, Phys. Rev. Lett. 94 (1) (2005) 017803.
[84] P. Guo, J. Du, Y. Bao, W. Meng, Real-time video recognition for assessing plastic viscosity of ultra-high-performance concrete (UHPC), Measurement 191 (2022) 110809.
[85] J. Du, S. Mahjoubi, Y. Bao, N. Banthia, W. Meng, Modeling mixing kinetics for large-scale production of Ultra-High-Performance Concrete: effects of temperature, volume, and mixing method, Construct. Build. Mater. 397 (2023) 132439.
[86] W. Meng, K.H. Khayat, Mechanical properties of ultra-high-performance concrete enhanced with graphite nanoplatelets and carbon nanofibers, Compos. B Eng. 107 (2016) 113–122.
[87] J. Flores, M. Kamali, A. Ghahremaninezhad, An investigation into the properties and microstructure of cement mixtures modified with cellulose nanocrystal, Materials 10 (5) (2017) 498.
[88] X.H. Wang, S. Jacobsen, J.Y. He, Z.L. Zhang, S.F. Lee, H.L. Lein, Application of nanoindentation testing to study of the interfacial transition zone in steel fiber reinforced mortar, Cement Concr. Res. 39 (8) (2009) 701–715.
[89] Z.-h. He, S.-g. Du, D. Chen, Microstructure of ultra high performance concrete containing lithium slag, J. Hazard Mater. 353 (2018) 35–43.
[90] G.-F. Peng, G. Zhang, H. Ding, Y.-J. Jia, Coating steel fiber for both CO2 capturing and strengthening of ultra-high performance concrete, J. Clean. Prod. 449 (2024) 141798.
[91] J. Huang, Y. Zhou, X. Yang, Y. Dong, M. Jin, J. Liu, A multi-scale study of enhancing mechanical property in ultra-high performance concrete by steel-fiber@Nano-silica, Construct. Build. Mater. 342 (2022) 128069.
[92] W.A. Zisman, Relation of the Equilibrium Contact Angle to Liquid and Solid Constitution, ACS Publications, 1964.
[93] Z. Lu, J. Yao, C.K.Y. Leung, Using graphene oxide to strengthen the bond between PE fiber and matrix to improve the strain hardening behavior of SHCC, Cement Concr. Res. 126 (2019) 105899.
[94] B. Han, L. Zhang, S. Zeng, S. Dong, X. Yu, R. Yang, J. Ou, Nano-core effect in nano-engineered cementitious composites, Compos. Appl. Sci. Manuf. 95 (2017) 100–109.

[95] X. Wang, S. Dong, A. Ashour, W. Zhang, B. Han, Effect and mechanisms of nanomaterials on interface between aggregates and cement mortars, Construct. Build. Mater. 240 (2020) 117942.
[96] X. Wang, S. Dong, Z. Li, B. Han, J. Ou, Nanomechanical characteristics of interfacial transition zone in nano-engineered concrete, Engineering 17 (2022) 99–109.
[97] J. Wang, S. Dong, C. Zhou, A. Ashour, B. Han, Investigating pore structure of nano-engineered concrete with low-field nuclear magnetic resonance, J. Mater. Sci. 56 (1) (2021) 243–259.
[98] W. Meng, K.H. Khayat, Improving flexural performance of ultra-high-performance concrete by rheology control of suspending mortar, Compos. B Eng. 117 (2017) 26–34.
[99] M.D. Abràmoff, P.J. Magalhães, S.J. Ram, Image processing with ImageJ, Biophot. Int. 11 (7) (2004) 36–42.
[100] L. Teng, H. Huang, J. Du, K.H. Khayat, Prediction of fiber orientation and flexural performance of UHPC based on suspending mortar rheology and casting method, Cement Concr. Compos. 122 (2021) 104142.
[101] L. Teng, H. Huang, K.H. Khayat, X. Gao, Simplified analytical model to assess key factors influenced by fiber alignment and their effect on tensile performance of UHPC, Cement Concr. Compos. 127 (2022) 104395.